Real-space calculations to obtain a quantitative understanding of the electronic structure of layered materials such as tBG, tNG, GBN and hBN encapsulated BG

Twistronics 2023

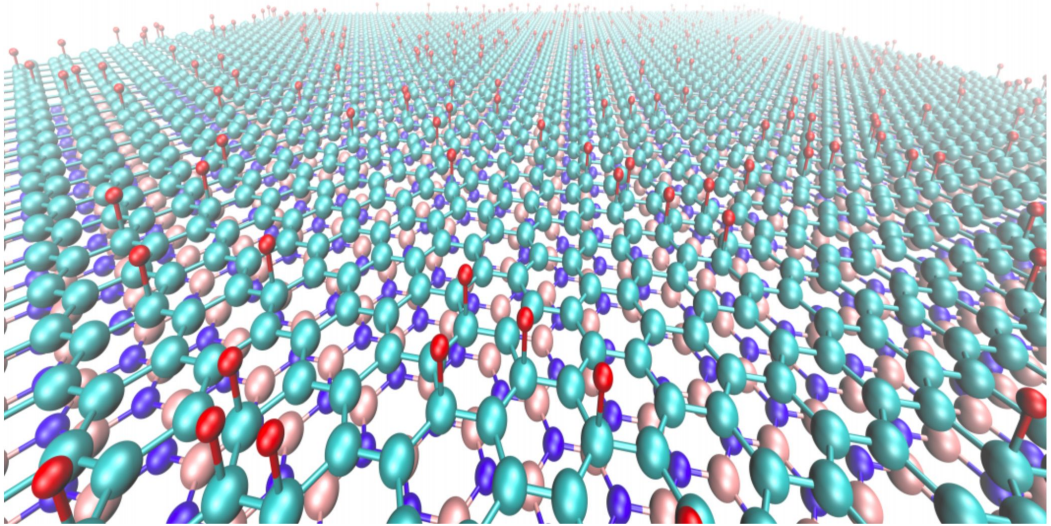

Advisor: Prof. GJ Jung
Collaborators: JQ An, YJ Park, S Javvaji, A Samudrala

Nicolas Leconte
University of Seoul

Direct observation of flat bands in twisted bilayer graphene

- Experimental ARPES observation
- Multi-scale approach to match experimental observations

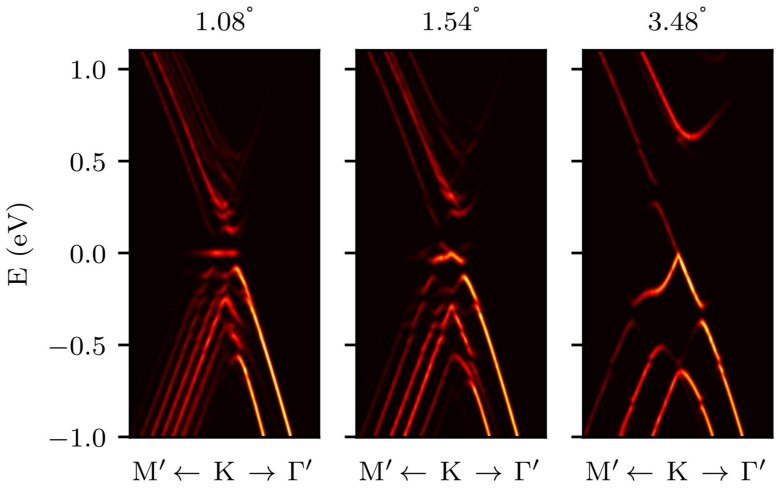

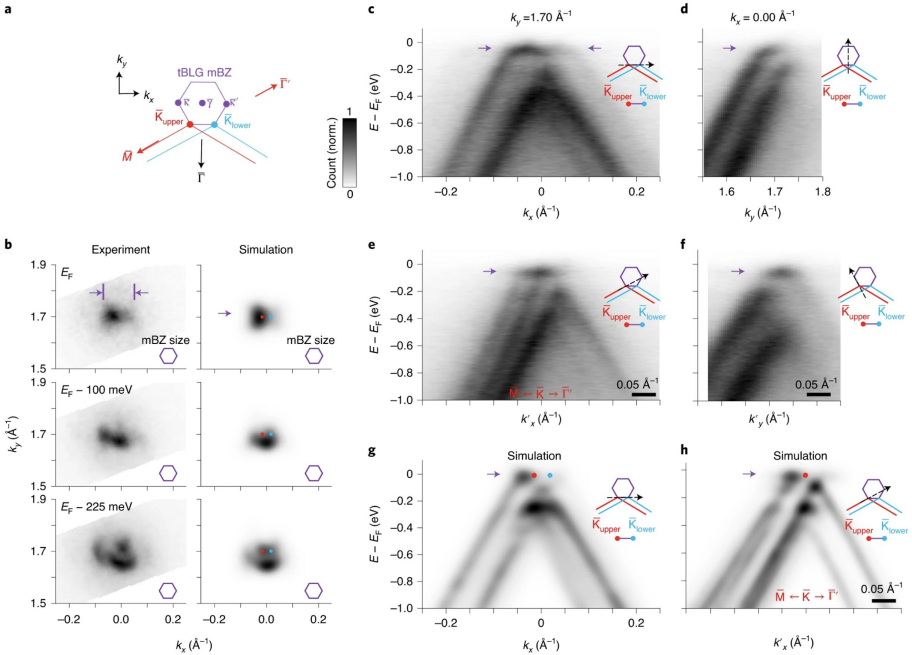

Visualization of the flat electronic band in twisted bilayer graphene near the magic angle twist

M. Iqbal Bakti Utama, Roland J. Koch, Kyunghoon Lee, Nicolas Leconte, Hongyuan Li, Sihan Zhao, Lili Jiang, Jiayi Zhu, Kenji Watanabe, Takashi Taniguchi, Paul D. Ashby, Alexander Weber-Bargioni, Alex Zettl, Chris Jozwiak, Jeil Jung, Eli Rotenberg, Aaron Bostwick and Feng Wang

Real-space multiscale methodology

Multi-scale approach

vdW physics with a covalent flavor: atoms try to hybridize to minimize their energies

Lattice reconstruction

Large systems: limited applicability of DFT

Classical energy minimizations and TB models to the rescue!

Develop an accurate force-field and simple TB model combination which reproduces experimental predictions quantitatively

Methodology

DFT calculations:

- Accuracy, computationally expensive
- Appropriate scheme (LDA, RPA, etc)
- For select number of commensurate stackings

KLIFF

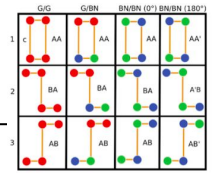

Classical potential fitting:

- Registry-dependent potentials (Kolmogorov-Crespi, Drip, ILP,...)
- Rebo, Tersoff,... intralayer potentials
- Machine learning potentials (Gap20)

(Accurate continuum models)

Real-space tight-binding (TB) model

Energy minimizations

- Use LAMMPS (or Gromacs, or…)
- Quantify relaxation effects such as lattice reconstruction, corrugation, etc

Large scale TB simulations:

- Compare rigid and relaxed structures
- Electronic band structure
- Spectral function
- Electronic transport

Relaxation effects in twisted bilayer graphene: A multiscale approach

Nicolas Leconte, Srivani Javvaji, Jiaqi An, Appalakondaiah Samudrala, and Jeil Jung
Phys. Rev. B **106**, 115410 – Published 12 September 2022

LAMMPS…

Pairwise potential

- Lennard-Jones

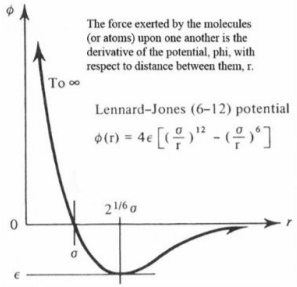

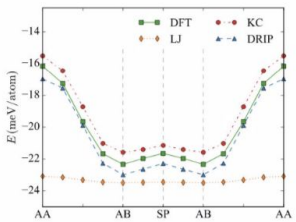

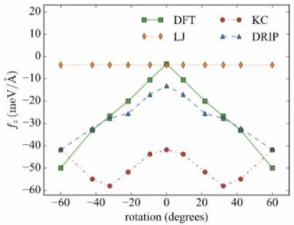

LAMMPS…

Pairwise potential

- Lennard-Jones

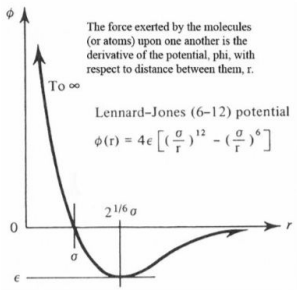

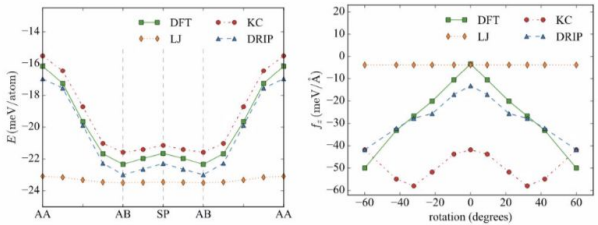

- Kolmogorov-Crespi

$$
\begin{aligned}
E &= \frac{1}{2}\sum_{i}\sum_{j\neq i} V_{ij} \\
V_{ij} &= e^{-\lambda(r_{ij}-z_0)}\left[C + f(\rho_{ij}) + f(\rho_{ji})\right] - A\left(\frac{r_{ij}}{z_0}\right)^{-6} + A\left(\frac{\text{cutoff}}{z_0}\right)^{-6} \\
\rho_{ij}^2 = \rho_{ji}^2 &= x_{ij}^2 + y_{ij}^2 \qquad (\mathbf{n_i} \equiv \hat{\mathbf{z}}) \\
f(\rho) &= e^{-(\rho/\delta)^2}\sum_{n=0}^{2} C_{2n}\left(\rho/\delta\right)^{2n}
\end{aligned}
$$

LAMMPS…

New drip parameters (also for G-BN and BN-BN interactions)

DRIP		C_0	C_2	C_4	C	δ	λ	A	z_0	B	η
EXX-RPA	CC	8.568E-03	1.781E-03	-3.277E-08	-4.616E-02	0.465	1.259	-4.049E-02	3.305	1.552E-02	-1.026
	CB	2.650E-02	5.326E-02	7.749E-02	4.037E-08	0.881	3.055	1.544E-08	3.133	8.052E-03	1.277
	CN	3.585E-02	1.710E-04	2.061E-02	7.224E-03	0.773	3.115	5.188E-02	3.084	4.222E-03	1.083
	BB	0.211	9.106E-02	3.252E-02	0.232	0.939	2.834	4.292E-08	2.735	3.324E-12	1.141
	BN	1.446E-06	0.108	0.186	1.085E-02	1.076	5.112	4.071E-08	2.871	7.748E-03	2.748
	NN	1.176E-02	4.701E-03	8.515E-03	4.293E-02	0.779	1.310	0.197	2.958	1.787E-03	2.073
LDA	CC	5.889E-02	2.150E-02	5.265E-02	1.601E-11	0.760	3.987	1.550E-02	2.988	1.181E-04	1.791
	CB	3.811E-02	3.606E-02	0.105	2.903E-06	0.875	5.291	3.243E-02	2.931	2.691E-03	1.147
	CN	6.882E-02	2.227E-02	3.967E-02	1.589E-07	0.743	3.007	7.131E-07	2.941	1.093E-02	1.268
	BB	0.274	0.142	3.252E-02	8.587E-07	0.696	3.121	9.474E-07	2.677	3.662E-10	1.120
	BN	8.727E-08	0.245	0.302	7.015E-02	1.225	5.929	5.785E-08	2.834	6.142E-03	2.950
	NN	2.002E-02	1.658E-02	1.182E-02	2.889E-03	0.774	1.323	0.159	2.535	1.111E-03	1.522

Pairwise potential

- Lennard-Jones

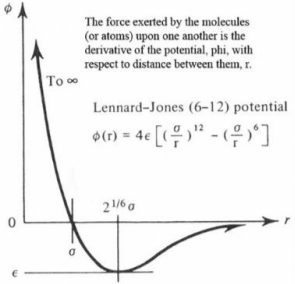

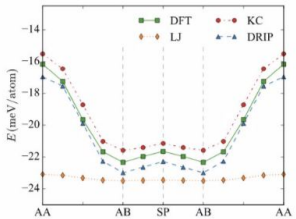

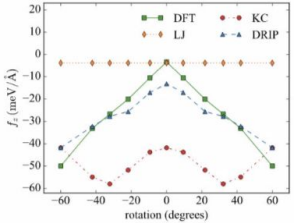

- Kolmogorov-Crespi

$$E = \frac{1}{2}\sum_i \sum_{j\neq i} V_{ij}$$

$$V_{ij} = e^{-\lambda(r_{ij}-z_0)}\left[C + f(\rho_{ij}) + f(\rho_{ji})\right] - A\left(\frac{r_{ij}}{z_0}\right)^{-6} + A\left(\frac{\text{cutoff}}{z_0}\right)^{-6}$$

$$\rho_{ij}^2 = \rho_{ji}^2 = x_{ij}^2 + y_{ij}^2 \qquad (\mathbf{n_i} \equiv \hat{\mathbf{z}})$$

$$f(\rho) = e^{-(\rho/\delta)^2}\sum_{n=0}^{2} C_{2n}\,(\rho/\delta)^{2n}$$

- DRIP (dihedral-angle-corrected registry-dependent) Potential

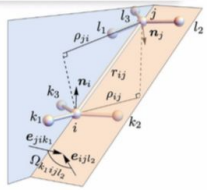

FIG. 2. Schematic representation of an atomic geometry that defines the normal vectors $\boldsymbol{n}_i$ and $\boldsymbol{n}_j$ and the dihedral angle $\Omega_{k_1ijl_2}$.

$$E = \frac{1}{2}\sum_i \sum_{j\notin \text{layer } i} \phi_{ij}$$

$$\phi_{ij} = f_c(x_r)\left[e^{-\lambda(r_{ij}-z_0)}\left[C + f(\rho_{ij}) + g(\rho_{ij}, \{\alpha_{ij}^{(m)}\})\right] - A\left(\frac{z_0}{r_{ij}}\right)^6\right]$$

Mingjian Wen, Stephen Carr, Shiang Fang, Efthimios Kaxiras, and Ellad B. Tadmor

PHYSICAL REVIEW B98, 235404 (2018)

TB models: interlayer and intralayer terms

Intralayer:

- Use F2G2 models to simulate intralayer terms of hBN, G, BG, etc systems
- Add moire induced-intralayer modifications of onsite energies and first-nearest neighbor hopping terms

Interlayer:

- Modified two center approximation models for interlayer hoppings

F2G2 Models

- Wannierization of the pi-orbitals centered around the carbon atoms…
- Long-range interactions are reduced to relatively short-range effective models that capture the DFT pi-bands

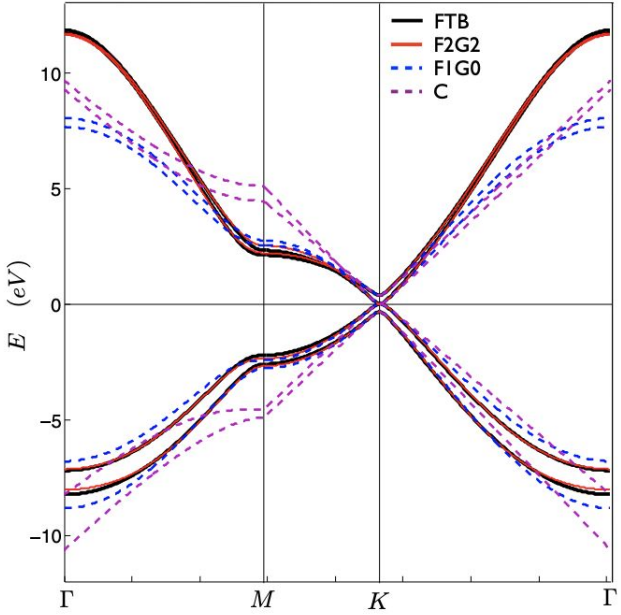

	t_{ABn}	$t_{AA'n}$	$t_{AB'n}$
f_1	−3.010	0.09244	0.1391
f_2	−0.1984	−0.02299	−0.07211
	t'_{AAn}	t'_{BBn}	$t'_{BA'n}$
g_0	0.4295	0.4506	0.3310
g_1	0.2235	0.2260	−0.01016
g_2	0.04016	0.0404	0.0001

PHYSICAL REVIEW B **89**, 035405 (2014)

Accurate tight-binding models for the π bands of bilayer graphene

Jeil Jung
Department of Physics, University of Texas at Austin, Austin, Texas 78712-0264, USA and Department of Physics, National University of Singapore, Singapore

Allan H. MacDonald
Department of Physics, University of Texas at Austin, Austin, Texas 78712-0264, USA
(Received 20 September 2013; revised manuscript received 12 December 2013; published 6 January 2014)

TB Hamiltonian

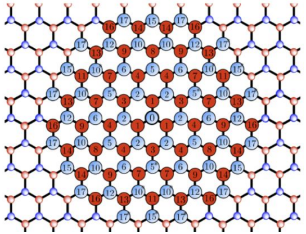

$$H = \boxed{H_{\text{intra}}} + H_{\text{inter}}.$$

TB Hamiltonian

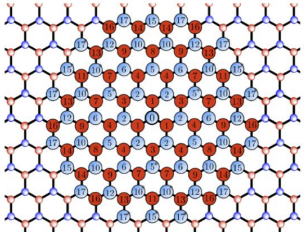

$$H = \boxed{H_{\text{intra}}} + H_{\text{inter}}.$$

$$H_{\text{intra}} = \boxed{H_{\text{intra}}^{\text{F2G2}}} + H_{\text{intra}}^{\text{virtual strain}}$$

Average from AA, AB and BA commensurate cell DFT calculations

t_{ij_n}	$C_1 - C_1$	$C_2 - C_2$	B-B	N-N		$C_1 - C_2$	B-N
g_0	-0.4017	-0.4027	2.3143	-1.7966			
g_1	0.24498	0.24523	0.081055	0.24562	f_1	-3.0307	-2.8928
g_2	0.06618	0.06624	0.065654	0.04892	f_2	-0.19334	-0.15399

$$H_{ii}(\boldsymbol{d}_{ij} : \mathbf{K}) = \sum_n t_{ii_n}(\boldsymbol{d}_{ij}) g_n(\mathbf{K})$$

$$H_{ij}(\boldsymbol{d}_{ij} : \mathbf{K}) = \sum_n t_{ij_n}(\boldsymbol{d}_{ij}) f_n(\mathbf{K})$$

TB Hamiltonian

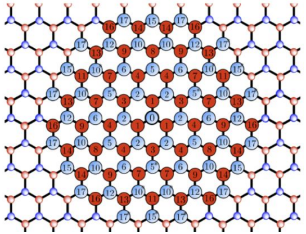

$$H = H_{\text{intra}} + H_{\text{inter}}.$$

$$H_{\text{intra}} = H_{\text{intra}}^{\text{F2G2}} + H_{\text{intra}}^{\text{virtual strain}}$$

Average from AA, AB and BA commensurate cell DFT calculations

t_{ij_n}	C_1-C_1	C_2-C_2	B-B	N-N		C_1-C_2	B-N
g_0	-0.4017	-0.4027	2.3143	-1.7966			
g_1	0.24498	0.24523	0.081055	0.24562	f_1	-3.0307	-2.8928
g_2	0.06618	0.06624	0.065654	0.04892	f_2	-0.19334	-0.15399

$$H_{ii}(\boldsymbol{d}_{ij} : \mathbf{K}) = \sum_n t_{ii_n}(\boldsymbol{d}_{ij}) g_n(\mathbf{K})$$

$$H_{ij}(\boldsymbol{d}_{ij} : \mathbf{K}) = \sum_n t_{ij_n}(\boldsymbol{d}_{ij}) f_n(\mathbf{K})$$

Moire bands

Take information from different local stacking configurations in the unit cell

Lattice mismatch Twist angle

$$\vec{d}_0(\vec{r}) \equiv \varepsilon\vec{r} + \theta\hat{z}\times\vec{r}$$

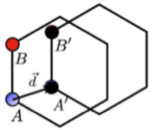

Moire periodicity $\vec{d}(\vec{r}+\vec{L}_M) = \vec{d}(\vec{r}) + \vec{L}$

From local stacking to moiré superlattices

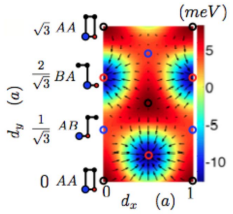

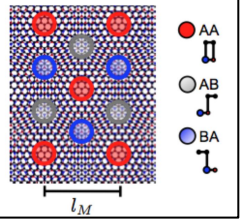

$$H_{\text{onsite}} = H_{ii} \quad \text{for} \quad g_0 = 1$$

$$H_{\text{onsite}}(\vec{d}) = C_{0ii} + 2C_{1ii}\,\mathrm{Re}\left[f(\vec{d})\exp(i\phi_{ii})\right]$$

$$ii = C_1, C_2, B \text{ or } N$$

$$f(\vec{d}) = \exp(-iG_1 d_y) + 2\exp\left(i\frac{G_1 d_y}{2}\right)\cos\left(\frac{\sqrt{3}}{2}G_1 d_x\right)$$

TB Hamiltonian

$$H = \boxed{H_{\text{intra}}} + H_{\text{inter}}.$$

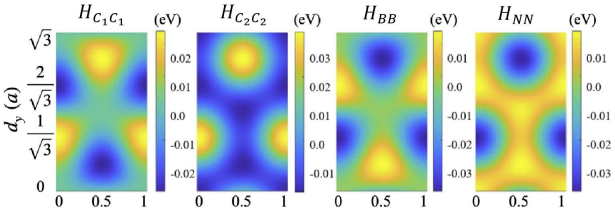

$$H_{\text{intra}} = \boxed{H_{\text{intra}}^{\text{F2G2}}} + H_{\text{intra}}^{\text{virtual strain}}$$

		a	b	c
$H_{C_1C_1}$	A	-0.770	0.589	-1.510
	B	-0.154	1.178	-2.641
	C	-0.028	1.125	-0.754
$H_{C_2C_2}$	A	-0.149	1.125	-2.513
	B	-0.121	0.940	-2.204
	C	0.030	-0.214	0.005
H_{BB}	A	-1.579	10.444	-19.057
	B	-0.972	6.388	-12.266
	C	-2.092	14.097	-25.568
H_{NN}	A	-0.468	3.278	-3.384
	B	-0.188	1.318	0.065
	C	-0.290	2.315	-2.208

$$A(B,C) = a\left(c^{\perp}\right)^2 + bc^{\perp} + c$$

$$D = (A-B)/(B-C)$$

$$\varphi_{ii} = \arctan\left[-\frac{\sqrt{3}}{2(D+1/2)}\right]$$

$$C_{1ii} = (C-B)/6\sqrt{3}\sin\varphi$$

$$C_{0ii} = -6C_1\cos\varphi + A$$

$$H_{\text{onsite}}(\vec{d}) = C_{0ii} + 2C_{1ii}\,\text{Re}\left[f(\vec{d})\exp(i\phi_{ii})\right]$$

$$f(\vec{d}) = \exp(-iG_1d_y) + 2\exp\left(i\frac{G_1d_y}{2}\right)\cos\left(\frac{\sqrt{3}}{2}G_1d_x\right)$$

	A	B	C	Average
C_1	-0.39969	-0.37776	-0.4277	-0.4017
C_2	-0.42011	-0.36739	-0.42048	-0.4027
B	2.3222	2.2731	2.3476	2.3143
N	-1.7795	-1.8324	-1.7778	-1.7966

TB Hamiltonian

$$H = \boxed{H_{\text{intra}}} + H_{\text{inter}}.$$

$$H_{\text{intra}} = H_{\text{intra}}^{\text{F2G2}} + \boxed{H_{\text{intra}}^{\text{virtual strain}}}$$

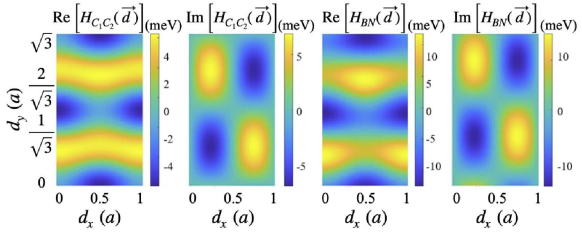

TB Hamiltonian

$$H = H_{\text{intra}} + H_{\text{inter}}.$$

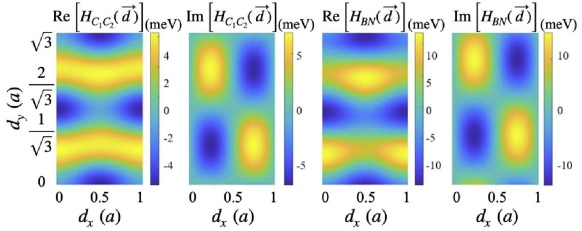

$$H_{\text{intra}} = H_{\text{intra}}^{\text{F2G2}} + H_{\text{intra}}^{\text{virtual strain}}$$

TB-mapping

$$H_{ij}(\vec{d}) = 2C_{ij}\cos\left(\frac{\sqrt{3}G_1}{2}d_x\right)\cos\left(\frac{G_1}{2}d_y - \varphi_{ij}\right) - 2C_{ij}\cos\left(G_1 d_y + \varphi_{ij}\right) - i2\sqrt{3}C_{ij}\sin\left(\frac{\sqrt{3}G_1}{2}d_x\right)\cos\left(\frac{G_1}{2}d_y - \varphi_{ij}\right)$$

$C_{ij} = 1.987$ meV and $\varphi_{ij} = 3.5°$

$C_{ij} = 4.418$ meV and $\varphi_{ij} = 26.10°$

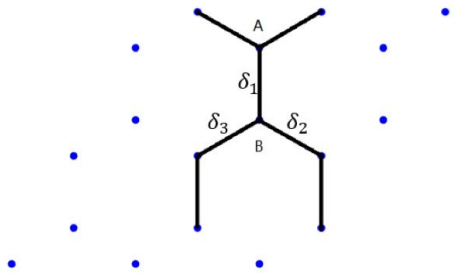

$$t = t_0 + \delta_i, \text{ i=1,2,3}$$

$$\delta_1 = 2A'/3, \delta_2 = -(A' + \sqrt{3}B')/3, \delta_3 = (-A' + \sqrt{3}B')/3$$

$$A' = \text{Re}(H_{ij}), B' = \text{Im}(H_{ij}).$$

TB Hamiltonian

$$H = H_{\text{intra}} + \boxed{H_{\text{inter}}}.$$

	p (Å)	q (Å)
$C_1 - B$	3.0477	1.0280
$C_1 - N$	3.4755	1.1922
$C_2 - B$	3.0646	1.0492
$C_2 - N$	3.4799	1.1622

$$t^{\text{inter}}_{\text{model},ij} = \exp\left[\frac{r_z - p}{q}\right] t^{\text{inter}}_{\text{TC},ij}$$

$$H_{ss'}(\boldsymbol{K} : \boldsymbol{d}) = \sum_{j_{s'}} t^{\text{inter}}_{i_s j_{s'}} \exp\left[\mathrm{i}\boldsymbol{K} \cdot (\boldsymbol{d} + \boldsymbol{r}_{i_s j_{s'}})\right]$$

$$t^{\text{inter}}_{\text{TC},ij} = V_{pp\pi}(r_{ij}) \left[1 - \left(\frac{r_z}{r_{ij}}\right)^2\right] + V_{pp\sigma}(r_{ij}) \left(\frac{r_z}{r_{ij}}\right)^2$$

$$V_{pp\pi}(r_{ij}) = V^0_{pp\pi} \exp\left(-\frac{r_{ij} - a_{\text{CC}}}{r_0}\right)$$

$$V_{pp\sigma}(r_{ij}) = V^0_{pp\sigma} \exp\left(-\frac{r_{ij} - c_0}{r_0}\right)$$

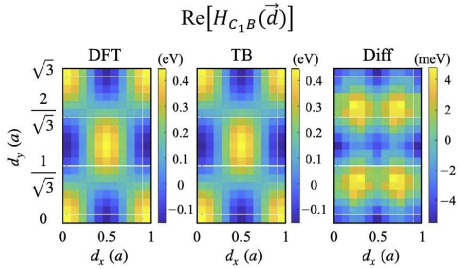

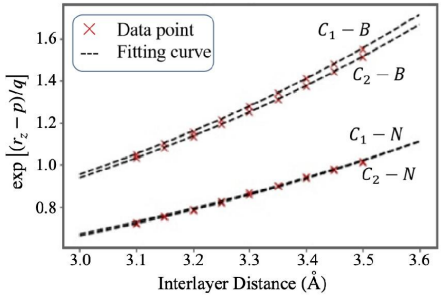

Magic angle renormalization in tBG

$$t_{\mathrm{SHE},ij} = \begin{cases} t^{\mathrm{intra}}_{\mathrm{F3G2},ij} & \text{if } i \in \text{ layer } j \\ S \exp\left[(c_{ij} - p)/q\right] t^{\mathrm{inter}}_{\mathrm{TC},ij} & \text{if } i \notin \text{ layer } j \end{cases}$$

Wide bracket of magic angles

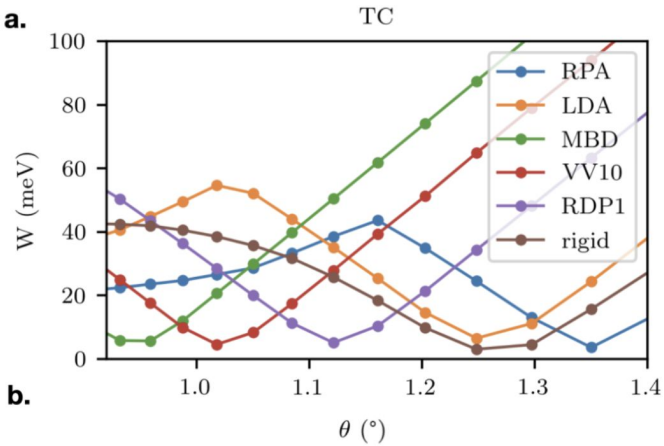

S	STC	SH	SHE
RPA	0.752	0.951	0.895
LDA	0.804	1.018	0.945
MBD	1.069	1.353	1.144
KC-VV10	0.970	1.247	1.091
KC-RDP1	0.884	1.136	1.018
Rigid	0.856	1.083	1.008

$$S = \frac{\theta_1 |t_{\mathrm{eff}}|}{\omega} s = C_1 s$$

$$S' = C_1' s = C_1 \left(1 + \frac{\delta\theta}{\theta_1}\right)\left(1 + \frac{\delta v_{\mathrm{F}}}{v_{\mathrm{F}}}\right)\left(\frac{\omega}{\omega + \delta\omega}\right)$$

Magic angle at chosen value

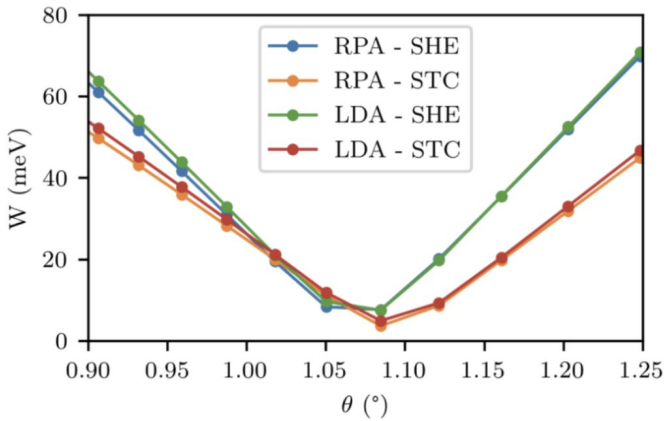

Intra-layer force field effect

Hybrid neural network potential for multilayer graphene

Mingjian Wen[1] and Ellad B. Tadmor[1,*]

[1] *Department of Aerospace Engineering and Mechanics, University of Minnesota, Minneapolis, MN 55455, USA*

(Dated: November 19, 2019)

Method	a (Å)	d_{AB} (Å)	d_{AA} (Å)	$d_{graphite}$ (Å)	E_{AB} (eV/atom)	E_{coh} (eV/atom)	E_v (eV)	C_{11} (GPa)	C_{12} (GPa)	C_{13} (GPa)	C_{33} (GPa)	C_{44} (GPa)	Time (relative)
hNN–Gr$_x$ (present)	2.467	3.457	3.618	3.402	21.63	8.07	8.08	978.31 (1061.83)	176.54 (208.77)	−66.74	40.35	1.79	279.4
AIREBO [20]	2.419	3.392	3.416	3.358	23.61	7.43	7.94	1153.50 (1162.46)	144.87 (147.64)	0.08	40.40	0.28	4.5
AIREBO–M [23]	2.420	3.299	3.324	3.294	16.18	7.42	7.93	1174.25 (1157.43)	147.66 (146.23)	-0.02	35.72	0.28	4.9
LCBOP [22]	2.459	3.346	3.365	3.346	12.52	7.35	8.13	1049.91 (1054.32)	157.29 (159.03)	0.04	29.80	0.23	1.6
ReaxFF [25]	2.462	3.285	3.294	3.260	34.59	7.52	7.52	1147.67 (1119.84)	831.84 (811.43)	−0.77	34.41	0.15	26.1
Tersoff [17]	2.530					7.39	7.12	(1274.00)	(−240.11)				1
REBO [19]	2.460					7.39	7.82	(1059.25)	(148.33)				1.6
GAP–Gr [38]	2.467					7.96	6.55	(1108.81)	(212.19)				3814.7
KC [12]		3.374	3.602	3.337	21.60						34.45		36.6
DRIP [26]		3.439	3.612	3.415	23.05						32.00		35.5
DFT(PBE+MBD)	2.466	3.426	3.641	3.400	22.63	8.06	7.93	1080.12 (1084.41)	162.25 (161.25)	−4.63	33.18	3.32	$\sim 10^7$
ACFDT–RPA		3.39[a]		3.34[b]							36[b]		
Experiment	2.46[c]			3.34[d]				1060[e] (1018[f])	180[e]	15[e]	36.5[e]	0.27[e]	
	2.46[g]			3.356[h]				1109[h]	139[h]	0[h]	38.7[h]	4.95[h]	

A Review on Mechanics and Mechanical Properties of 2D Materials – Graphene and Beyond

Deji Akinwande[1], Christopher J. Brennan[1], J. Scott Bunch[2], Philip Egberts[3], Jonathan R. Felts[4], Huajian Gao[5], Rui Huang[6*], Joon-Seok Kim[1], Teng Li[7], Yao Li[8], Kenneth M. Liechti[6*], Nanshu Lu[6], Harold S. Park[2], Evan J. Reed[9], Peng Wang[6], Boris I. Yakobson[10], Teng Zhang[11], Yong-Wei Zhang[12], Yao Zhou[9], Yong Zhu[13]

Table I. Linearly elastic properties of monolayer graphene predicted by first principles and empirical potential based calculations.

Method	2D Young's modulus Y_{2D} (N/m)	Poisson's ratio	Biaxial modulus (N/m)	Bending modulus D_m (eV)	Gaussian modulus D_G (eV)
DFT [46]	345	0.149	406	1.49	-
DFT [48]	348	0.169	419	-	-
DF-TB [44]	-	-	-	1.61	-0.7
DFT [58]	-	-	-	1.44	-1.52
REBO-1 [51]	236	0.412	401	0.83	-
REBO-2 [52]	243	0.397	403	1.41	-
AIREBO [53]	279	0.357	434	1.56	-
REBO-LB [56]	349	0.132	402	-	-
LCBOPII [59]	343	0.156	406	~1.1	-

Improved intra-layer with EXX-RPA informed interlayer

An accurate and transferable machine learning potential for carbon

J. Chem. Phys. **153**, 034702 (2020); https://doi.org/10.1063/5.0005084

Patrick Rowe[1], Volker L. Deringer[2], Piero Gasparotto[1], Gábor Csányi[3], *and* Angelos Michaelides[1,a)]

Naturally recover flat band at 1.08°

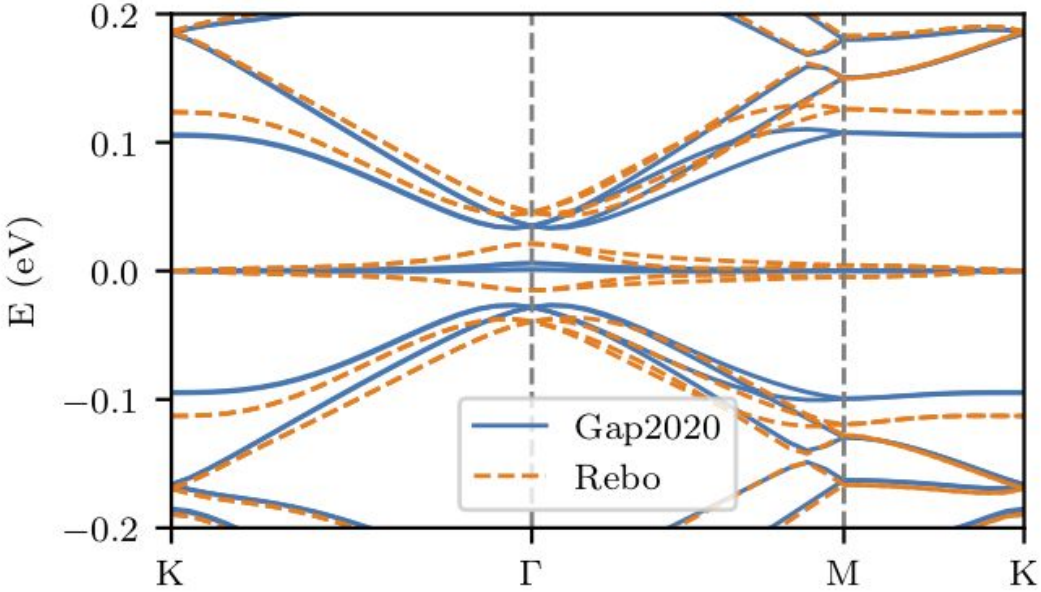

Building the commensurate cell

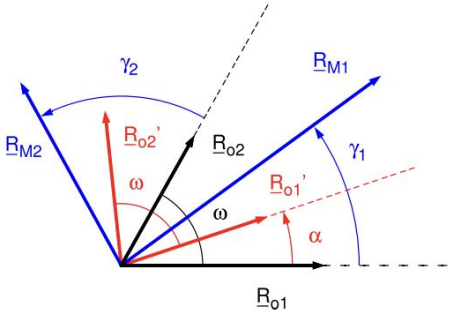

Figure 2. Definition of lattice vectors and angles of the substrate, $\underline{R}_{o1}$, $\underline{R}_{o2}$, ω, of the overlayer, $\underline{R}'_{o1}$, $\underline{R}'_{o2}$, and of the moiré lattice, $\underline{R}_{M1}$, $\underline{R}_{M2}$, γ_1, γ_2.

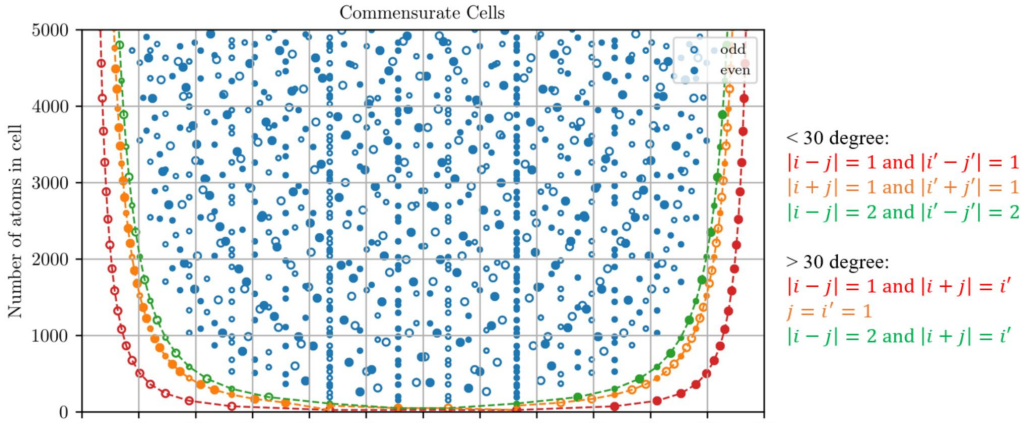

$$M = \begin{pmatrix} a & b \\ -b & a+b \end{pmatrix}, M' = \begin{pmatrix} a' & b' \\ -b' & a'+b' \end{pmatrix}, \begin{pmatrix} R_1 \\ R_2 \end{pmatrix} = M \begin{pmatrix} R_{o1} \\ R_{o2} \end{pmatrix} = M' \begin{pmatrix} R'_{o1} \\ R'_{o2} \end{pmatrix}$$

$$\cos(\alpha) = \frac{1}{2p\Gamma}\left[2a'a + 2b'b + a'b + b'a\right] \quad p = \sqrt{\frac{a'^2 + b'^2 + a'b'}{a^2 + b^2 + ab}}$$

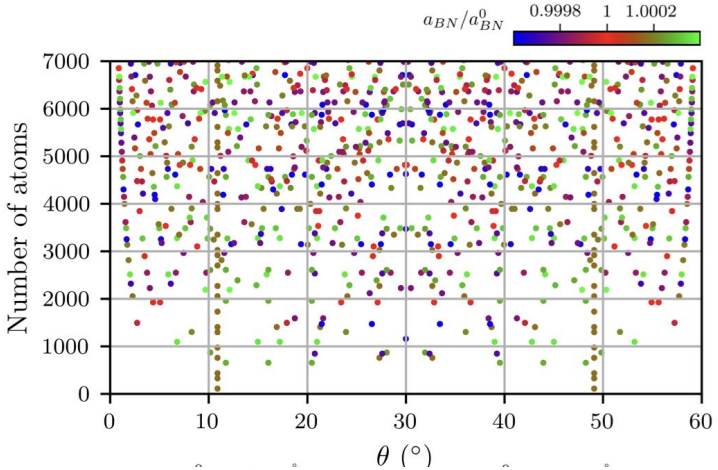

[1] K. Hermann, Journal of Physics: Condensed Matter 24, 314210 (2012).

Supermoire commensurate cells (e.g. hBN encapsulated BG)

$$\begin{pmatrix}\mathbf{r}_1\\ \mathbf{r}_2\end{pmatrix} = \mathbf{M}_1 \cdot \begin{pmatrix}\mathbf{a}_1\\ \mathbf{a}_2\end{pmatrix} = \mathbf{M}_{2/3} \cdot \begin{pmatrix}\mathbf{a}_1'\\ \mathbf{a}_2'\end{pmatrix} = \mathbf{M}_4 \cdot \begin{pmatrix}\mathbf{a}_1''\\ \mathbf{a}_2''\end{pmatrix}$$

$$\boldsymbol{M}_1 = \begin{pmatrix} i & j \\ -j & i+j \end{pmatrix},$$

$$\boldsymbol{M}_{2/3} = \begin{pmatrix} i' & j' \\ -j' & i'+j' \end{pmatrix},$$

$$\boldsymbol{M}_4 = \begin{pmatrix} i'' & j'' \\ -j'' & i''+j'' \end{pmatrix}.$$

$$\alpha_{12} = \frac{|\mathbf{a}_1|}{|\mathbf{a}_1'|} = \sqrt{\frac{i'^2 + j'^2 + i'j'}{i^2 + j^2 + ij}},$$

$$\alpha_{43} = \frac{|\mathbf{a}_1''|}{|\mathbf{a}_1'|} = \sqrt{\frac{i'^2 + j'^2 + i'j'}{i''^2 + j''^2 + i''j''}},$$

$$\theta_{12} = \theta_1 - \theta_2 = \cos^{-1}\left[\frac{2ii' + 2jj' + ij' + ji'}{2\alpha_{12}(i^2 + j^2 + ij)}\right],$$

$$\theta_{43} = \theta_4 - \theta_3 = \cos^{-1}\left[\frac{2i''i' + 2j''j' + i''j' + j''i'}{2\alpha_{43}(i''^2 + j''^2 + i''j'')}\right]$$

Electronic structure of lattice relaxed alternating twist tNG-multilayer graphene

Experiments

Published: 05 March 2018

Unconventional superconductivity in magic-angle graphene superlattices

Yuan Cao, Valla Fatemi, Shiang Fang, Kenji Watanabe, Takashi Taniguchi, Efthimios Kaxiras & Pablo Jarillo-Herrero

Nature **556**, 43–50 (2018) | Cite this article

187k Accesses | **2594** Citations | **638** Altmetric | Metrics

nature materials

ARTICLES

https://doi.org/10.1038/s41563-022-01287-1

Check for updates

Robust superconductivity in magic-angle multilayer graphene family

Jeong Min Park[1,3], Yuan Cao[1,3], Li-Qiao Xia[1], Shuwen Sun[1], Kenji Watanabe[2], Takashi Taniguchi[2] and Pablo Jarillo-Herrero[1]

Article

Tunable strongly coupled superconductivity in magic-angle twisted trilayer graphene

https://doi.org/10.1038/s41586-021-03192-0

Received: 26 October 2020

Accepted: 5 January 2021

Published online: 01 February 2021

Check for updates

Jeong Min Park[1,4], Yuan Cao[1,4], Kenji Watanabe[2], Takashi Taniguchi[3] & Pablo Jarillo-Herrero[1]

Moiré superlattices[1,2] have recently emerged as a platform upon which correlated physics and superconductivity can be studied with unprecedented tunability[3–6]. Although correlated effects have been observed in several other moiré systems[7–17], magic-angle twisted bilayer graphene remains the only one in which robust superconductivity has been reproducibly measured[4–6]. Here we realize a moiré superconductor in magic-angle twisted trilayer graphene (MATTG)[18], which has better tunability of its electronic structure and superconducting properties than magic-angle twisted bilayer graphene. Measurements of the Hall effect and quantum oscillations as a function of density and electric field enable us to determine the tunable phase boundaries of the system in the normal metallic state. Zero-magnetic-field resistivity measurements reveal that the existence of superconductivity is intimately connected to the broken-symmetry phase that emerges from two carriers per moiré unit cell. We find that the superconducting phase is suppressed and bounded at the Van Hove singularities that partially surround the broken-symmetry phase, which is difficult to reconcile with weak-coupling Bardeen–Cooper–Schrieffer theory. Moreover, the extensive in situ tunability of our system allows us to reach the ultrastrong-coupling regime, characterized by a Ginzburg–Landau coherence length that reaches the average inter-particle distance, and very large T_{BKT}/T_f values, in excess of 0.1 (where T_{BKT} and T_f are the Berezinskii–Kosterlitz–Thouless transition and Fermi temperatures, respectively). These observations suggest that MATTG can be electrically tuned close to the crossover to a two-dimensional Bose–Einstein condensate. Our results establish a family of tunable moiré superconductors that have the potential to revolutionize our fundamental understanding of and the applications for strongly coupled superconductivity.

REPORT

Electric field–tunable superconductivity in alternating-twist magic-angle trilayer graphene

Zeyu Hao[1,*], A. M. Zimmerman[1,*], Patrick Ledwith[1], Eslam Khalaf[1], Danial Haie Najafabadi[1], Kenji Watanabe[2], Takashi Taniguchi[3], Ashvin Vishwanath[1], Philip Kim[1,†]

[1]Department of Physics, Harvard University, Cambridge, MA 02138, USA.

[2]Research Center for Functional Materials, National Institute for Material Science, 1-1 Namiki, Tsukuba 305-0044, Japan.

[3]International Center for Materials Nanoarchitectonics, National Institute for Material Science, 1-1 Namiki, Tsukuba 305-0044, Japan.

↵†Corresponding author. Email: pkim@physics.harvard.edu

↵* These authors contributed equally to this work.

– Hide authors and affiliations

Science 12 Mar 2021:
Vol. 371, Issue 6534, pp. 1133-1138
DOI: 10.1126/science.abg0399

System

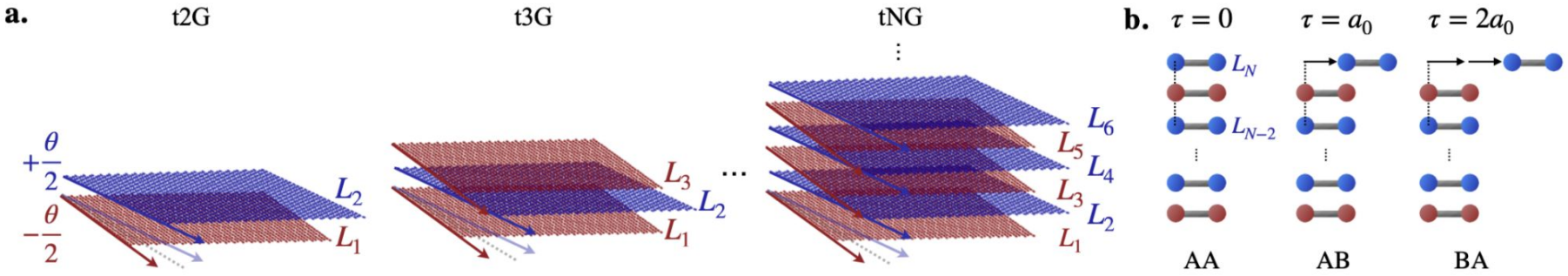

- Alternating twists
- Sliding between layers N and N-2

PAPER • OPEN ACCESS

Electronic structure of lattice relaxed alternating twist t*N*G-multilayer graphene: from few layers to bulk AT-graphite

Nicolas Leconte[1], Youngju Park[1], Jiaqi An[1], Appalakondaiah Samudrala[1,2] and Jeil Jung[1,3]

Published 31 August 2022 • © 2022 The Author(s). Published by IOP Publishing Ltd

2D Materials, Volume 9, Number 4

Focus on Twistronics in 2D Materials

Citation Nicolas Leconte *et al* 2022 *2D Mater.* **9** 044002

2 questions

- Energetic stability?

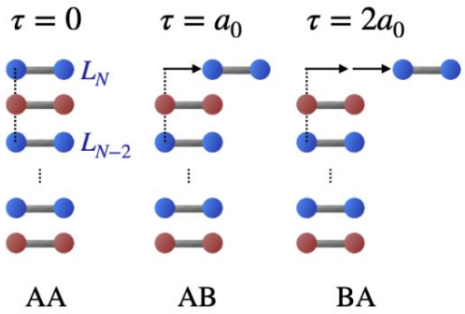

- Accuracy of analytical magic angle predictions?

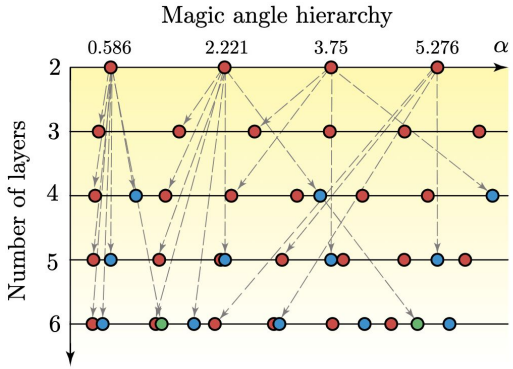

Editors' Suggestion

Magic angle hierarchy in twisted graphene multilayers

Eslam Khalaf, Alex J. Kruchkov, Grigory Tarnopolsky, and Ashvin Vishwanath
Phys. Rev. B **100**, 085109 – Published 2 August 2019

Stability: locked into double commensurate AA-stacking

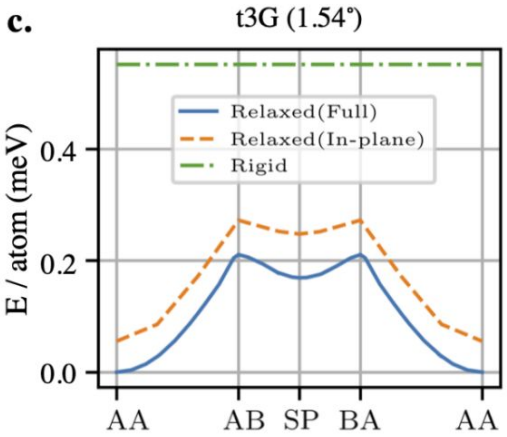

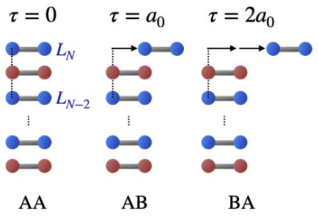

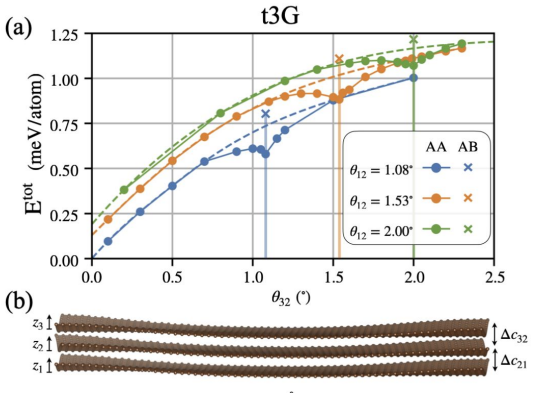

See Talk by Prof. G.J. Jung: Commensuration torques and lubricity in double moire systems

arXiv > cond-mat > arXiv:2301.04105

Condensed Matter > Mesoscale and Nanoscale Physics

[Submitted on 10 Jan 2023]

Commensuration torques and lubricity in double moire systems

Nicolas Leconte, Youngju Park, Jiaqi An, Jeil Jung

Editors' Suggestion

Magic angle hierarchy in twisted graphene multilayers

Eslam Khalaf, Alex J. Kruchkov, Grigory Tarnopolsky, and Ashvin Vishwanath
Phys. Rev. B **100**, 085109 – Published 2 August 2019

Magic angle numerical estimation: method

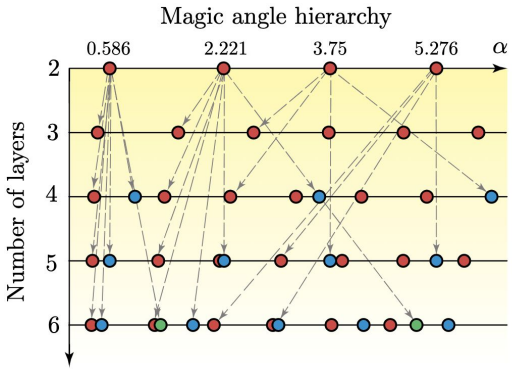

$$\theta^{(N)} = \omega/(v_F k_D \alpha_k^{(N)}) \qquad \alpha_k^{(N)} = \alpha^{(2)}/\lambda_k$$

$$t_{\mathrm{SHE},ij} = \begin{cases} t^{\mathrm{intra}}_{\mathrm{F3G2},ij} & \text{if } i \in \text{ layer } j \\ S \exp\left[(c_{ij} - p)/q\right] t^{\mathrm{inter}}_{\mathrm{TC},ij} & \text{if } i \notin \text{ layer } j \end{cases}$$

- Fix t2G magic angle at 1.08 degree using S
- Analytically estimate first magic for N>2 based on t2G coupling strength
- Calculate DOS for range of magic angles around this estimate (Lanczos recursion to tackle very large commensurate cells)
- Extract magic angle where DOS is largest`

Extracting the magic angle from DOS calculations

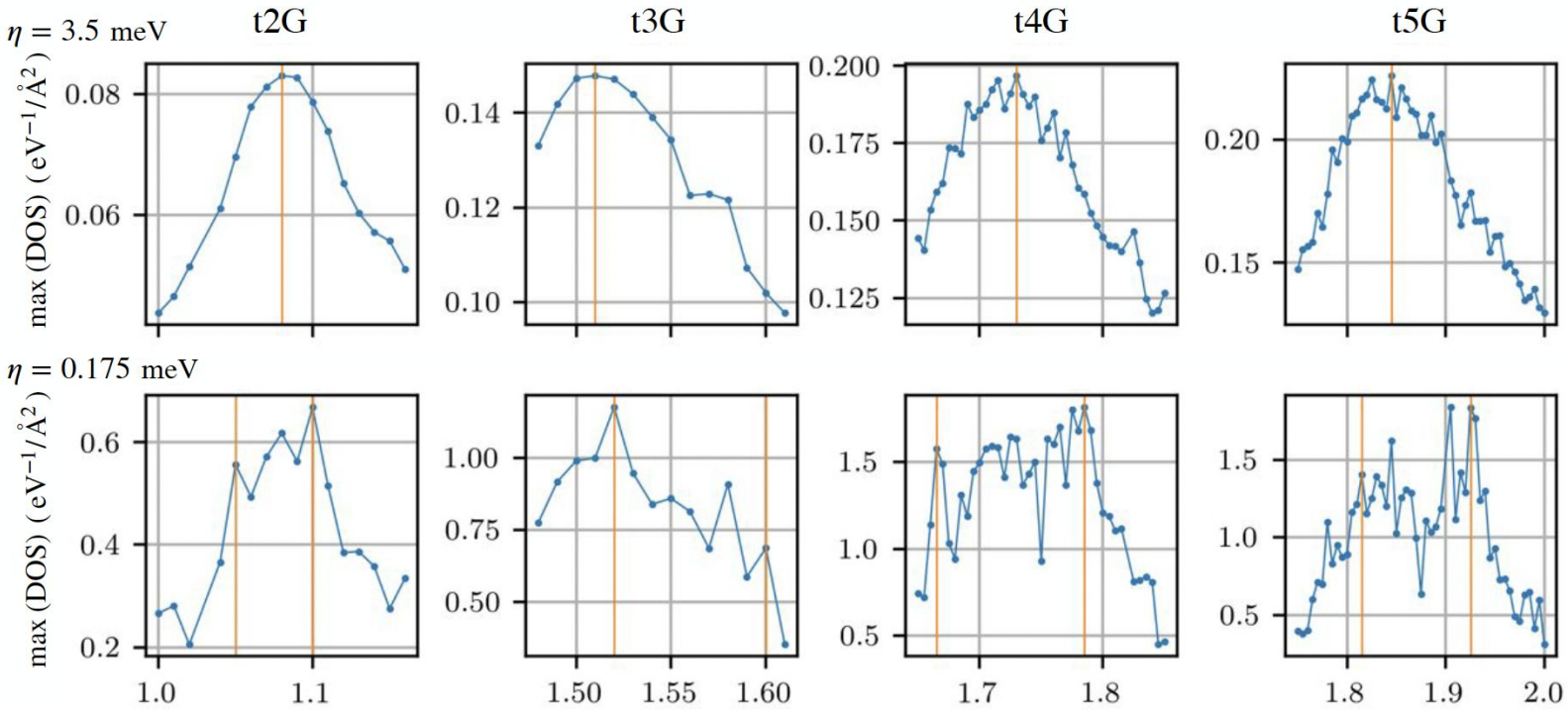

Magic angle reduction due to relaxation effects…

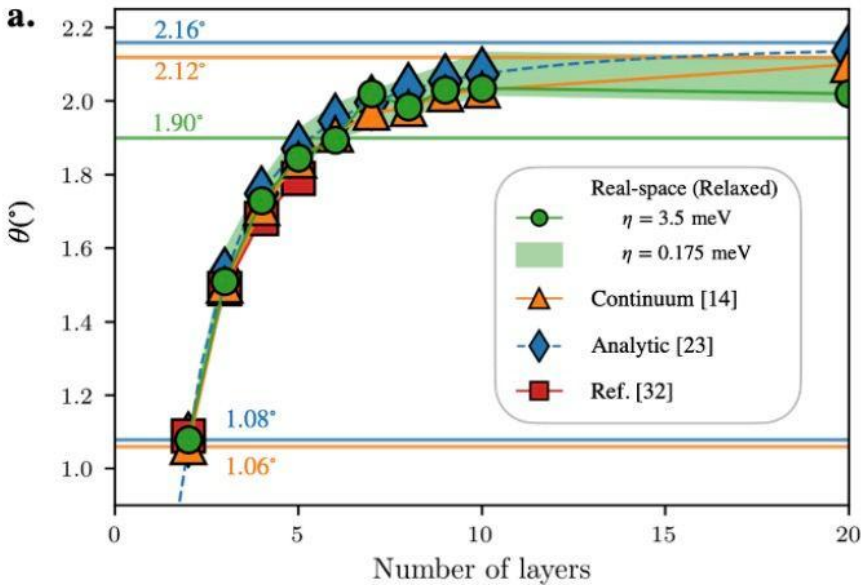

- Numerical magic angle (green) smaller than t2G-informed magic angle predictions (blue)
- Why…?

$$\kappa = w^{ij}_{\mathrm{AA}} / w^{ij}_{\mathrm{AB}}.$$

$$T(\boldsymbol{r}) = \sum_{j=0,\pm} e^{-i\boldsymbol{Q}_j\cdot\boldsymbol{r}} \left[\begin{pmatrix} \omega' & \omega\, e^{-i\phi_j} \\ \omega\, e^{i\phi_j} & \omega' \end{pmatrix} e^{-i\boldsymbol{G}_j\cdot\boldsymbol{\tau}_s} \right]$$

$$\omega_{XX'}(\boldsymbol{G}_j) = H_{XX'}(\boldsymbol{K}:\boldsymbol{G}_j) = \frac{1}{A_M}\int_{A_M} d\boldsymbol{r}\, \left[e^{i\boldsymbol{G}_j\cdot\boldsymbol{d}(\boldsymbol{r})}\, H_{XX'}(\boldsymbol{K}:\boldsymbol{d}(\boldsymbol{r})) \right]$$

Magic angle reduction: explanation

$$\alpha_k^{(n)} = \alpha^{(2)} / \left(2\cos\frac{\pi k}{n+1} \right) \qquad \alpha_i = w_{\mathrm{AB}} / (v_F k_D \theta_i)$$

- Reduced AB' coupling strength (see red dotted line) when increasing twist angle (reduced lattice reconstruction)
- Magic angle happens at larger angle for larger N

Weaker coupling implies magic angle reduction

(In-plane relaxation degree of freedom contributes primarily)

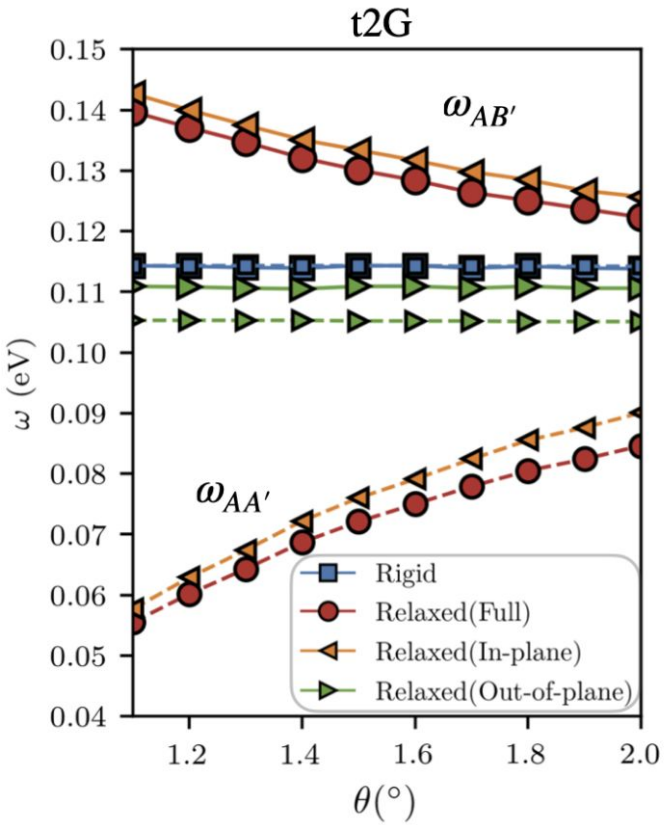

Take home message:

Reduction of magic angle values in tNG due to (in-plane) relaxation effects

PAPER • OPEN ACCESS

Electronic structure of lattice relaxed alternating twist t*NG*-multilayer graphene: from few layers to bulk AT-graphite

Nicolas Leconte[1], Youngju Park[1], Jiaqi An[1], Appalakondaiah Samudrala[1,2] and Jeil Jung[1,3]

Published 31 August 2022 • © 2022 The Author(s). Published by IOP Publishing Ltd

2D Materials, Volume 9, Number 4

Focus on Twistronics in 2D Materials

Citation Nicolas Leconte *et al* 2022 *2D Mater.* **9** 044002

Effect of substrate
on primary and secondary gaps in G on hBN

Motivation

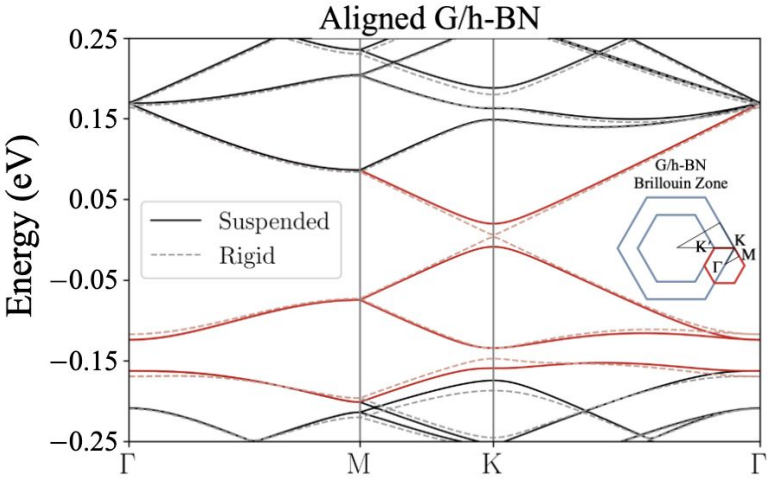

Ab initio theory of moiré superlattice bands in layered two-dimensional materials

Jeil Jung, Arnaud Raoux, Zhenhua Qiao, and A. H. MacDonald
Phys. Rev. B **89**, 205414 – Published 12 May 2014

Moiré band model and band gaps of graphene on hexagonal boron nitride

Jeil Jung, Evan Laksono, Ashley M. DaSilva, Allan H. MacDonald, Marcin Mucha-Kruczyński, and Shaffique Adam
Phys. Rev. B **96**, 085442 – Published 30 August 2017

Origin of band gaps in graphene on hexagonal boron nitride

Jeil Jung, Ashley M. DaSilva, Allan H. MacDonald & Shaffique Adam

Nature Communications **6**, Article number: 6308 (2015) | Cite this article

Effective lattice model of graphene moiré superlattices on hexagonal boron nitride

Xianqing Lin and Jun Ni
Phys. Rev. B **100**, 195413 – Published 12 November 2019

NANO LETTERS — Letter
Cite This: *Nano Lett.* 2018, 18, 7732−7741 — pubs.acs.org/NanoLett

Accurate Gap Determination in Monolayer and Bilayer Graphene/*h*-BN Moiré Superlattices

Hakseong Kim,[†,§] Nicolas Leconte,[‡,§] Bheema L. Chittari,[‡] Kenji Watanabe,[∥] Takashi Taniguchi,[∥] Allan H. MacDonald,[⊥] Jeil Jung,[*,‡] and Suyong Jung[*,†]

System

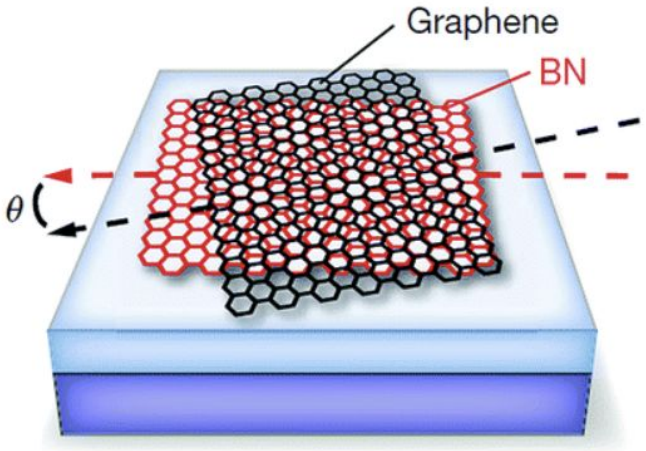

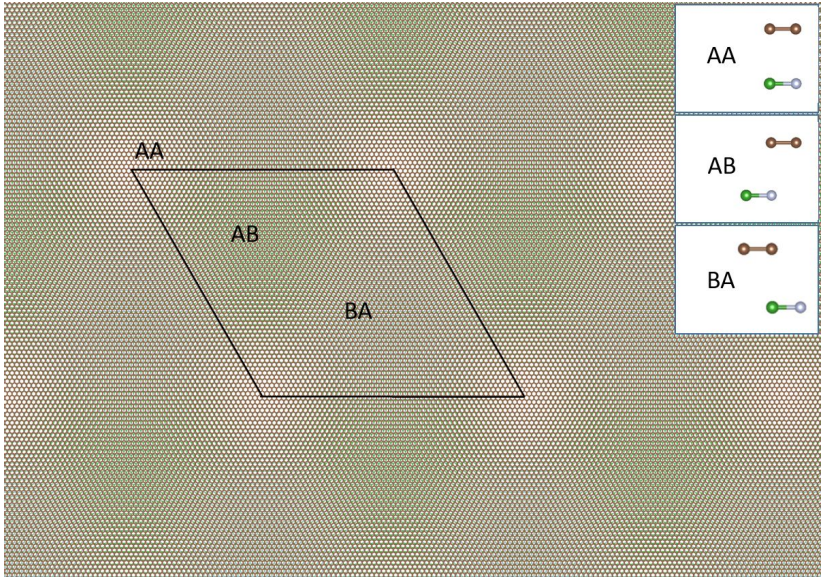

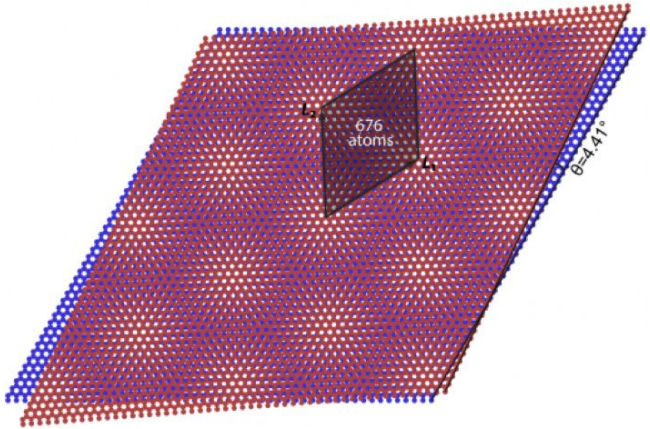

Primary and secondary gap: low angle regime

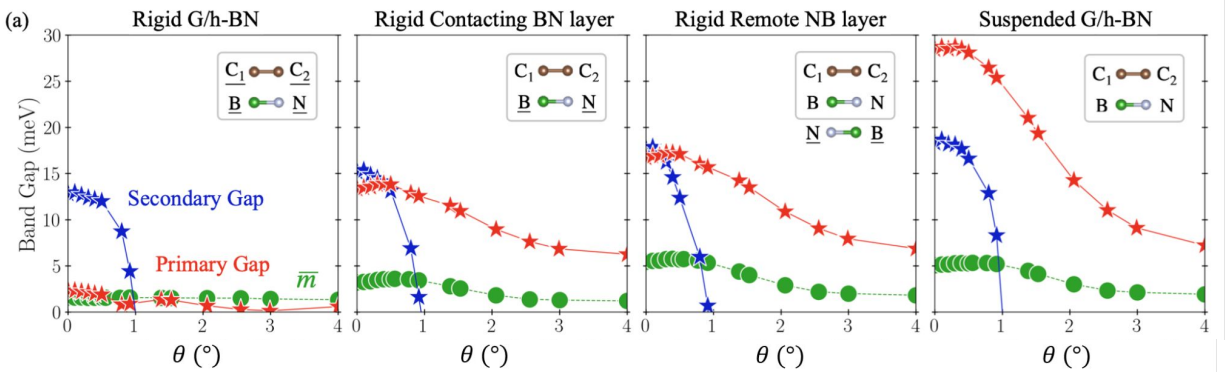

- Zero alignment: suspended G/h-BN shows largest gaps
- Increased rigidication of system: weak secondary gap reduction, large primary gap reduction
- Small increase of primary gap around 0.5 degree
- Relatively weak contribution of average mass-term gap to global gap value

Relaxation effects to explain the gap increase

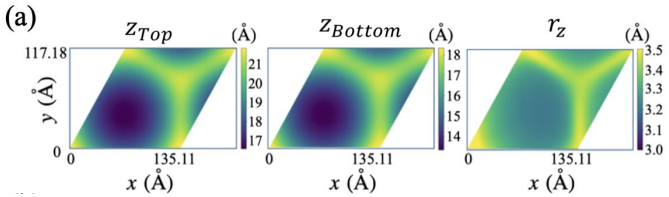

Relaxation effects to explain the gap increase

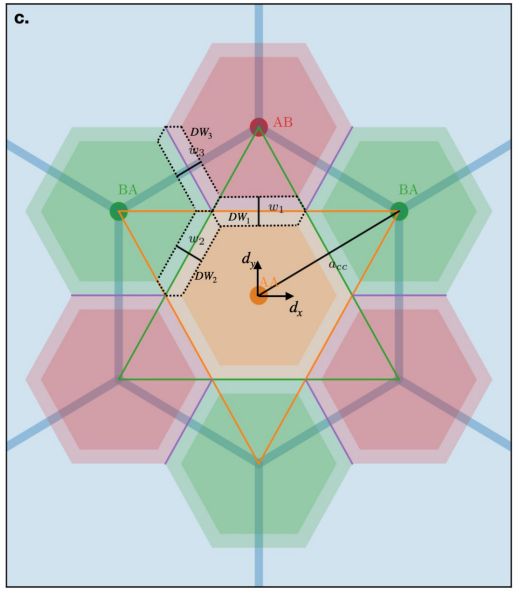

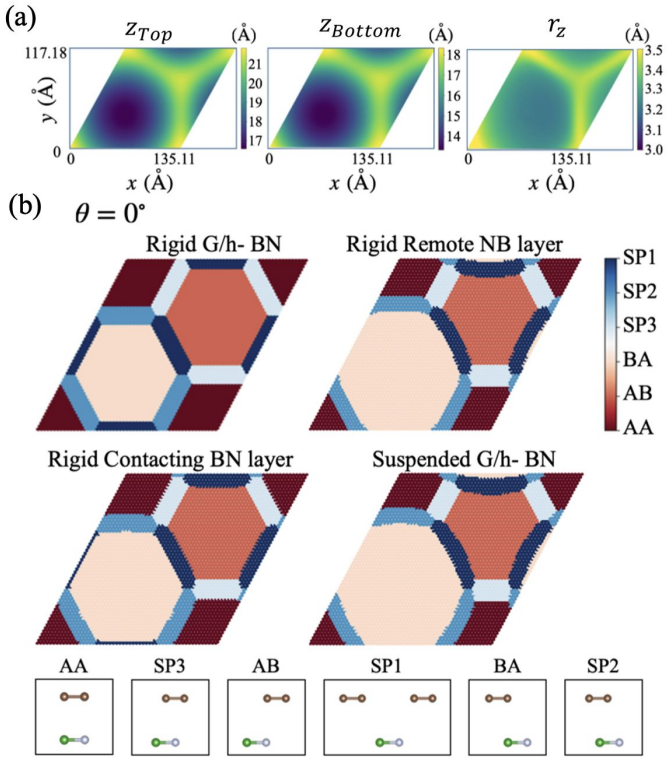

Relaxation effects to explain the gap increase

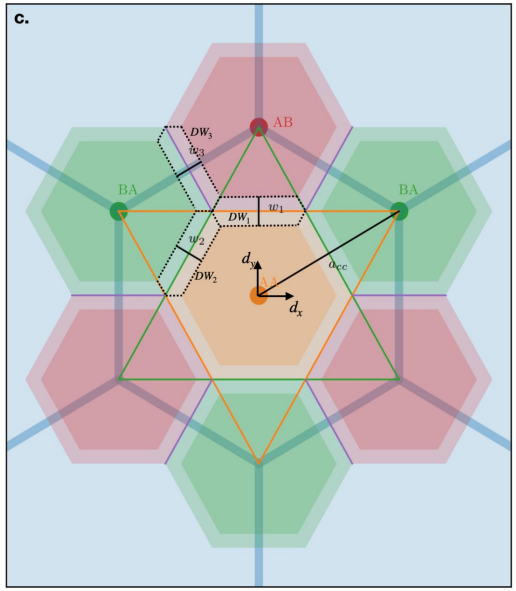

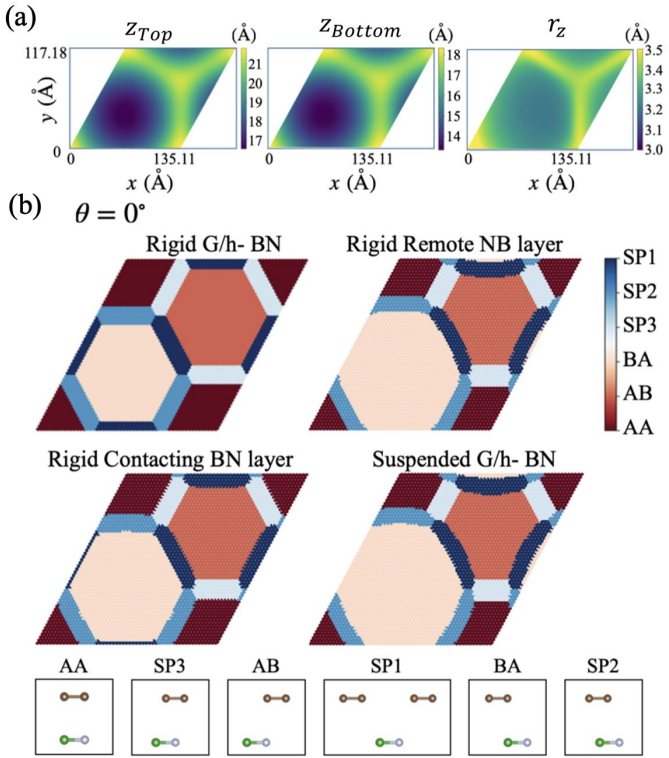

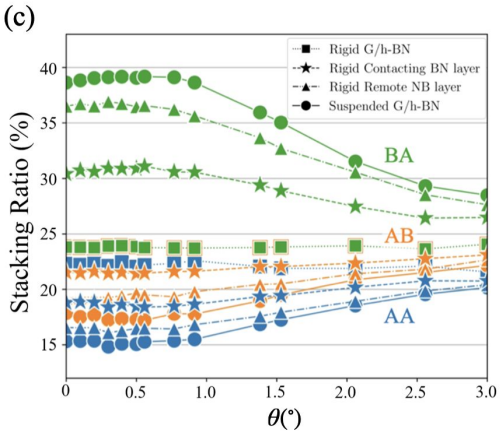

Relaxation effects to explain the gap increase

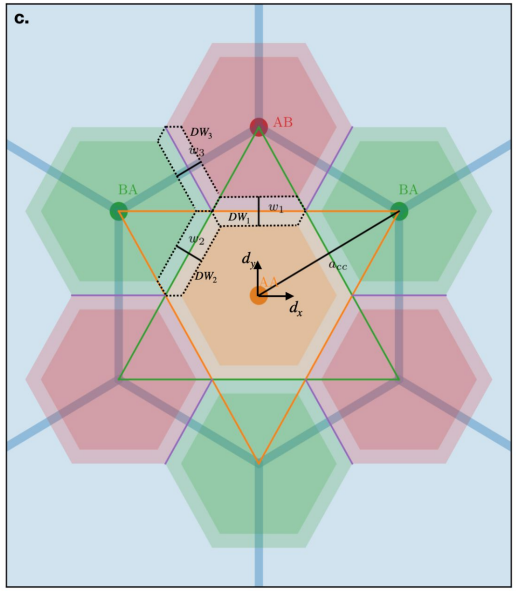

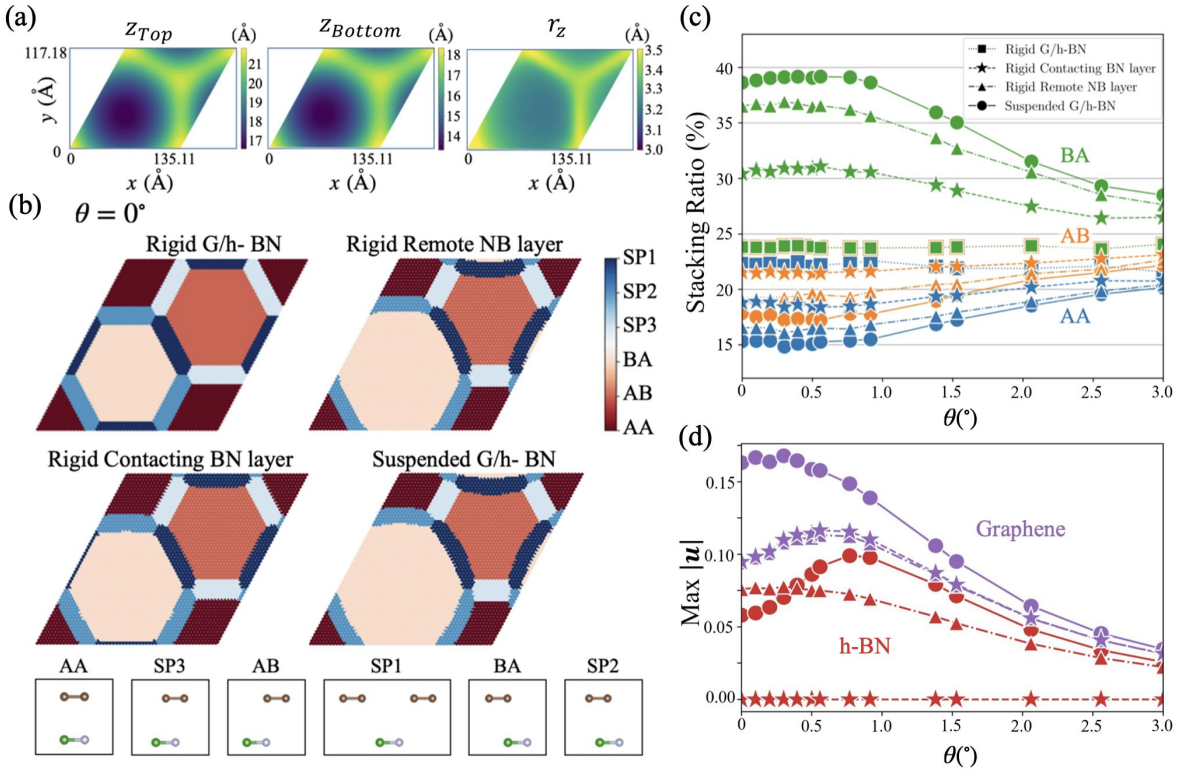

Understanding the primary gap increase: local rotation angle

$$\theta_R = s_{yx} - s_{xy}$$

$$s_{xy} = \frac{\partial u_x}{\partial y}$$

$$s_{yx} = \frac{\partial u_y}{\partial x}$$

Simple shear strain

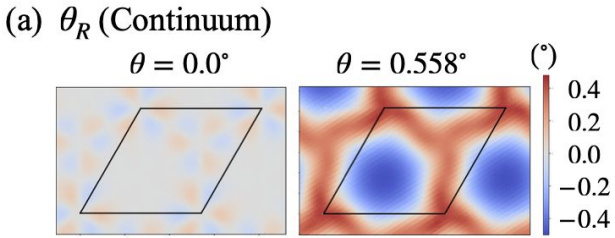

Red: against global rotation
Blue: with global rotation

Strain fields in twisted bilayer graphene

Nathanael P. Kazmierczak, Madeline Van Winkle, Colin Ophus, Karen C. Bustillo, Stephen Carr, Hamish G. Brown, Jim Ciston, Takashi Taniguchi, Kenji Watanabe & D. Kwabena Bediako

Nature Materials **20**, 956–963 (2021) | Cite this article

Understanding the primary gap increase: local rotation angle

$$\theta_R = s_{yx} - s_{xy}$$

$$s_{xy} = \frac{\partial u_x}{\partial y}$$

$$s_{yx} = \frac{\partial u_y}{\partial x}$$

Simple shear strain

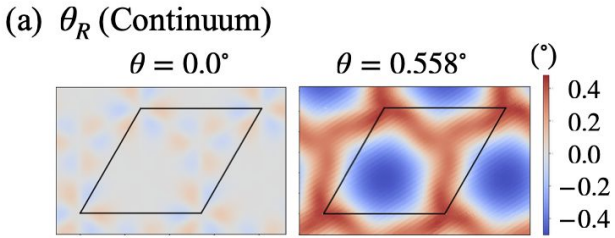

Red: against global rotation
Blue: with global rotation

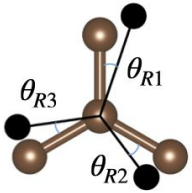

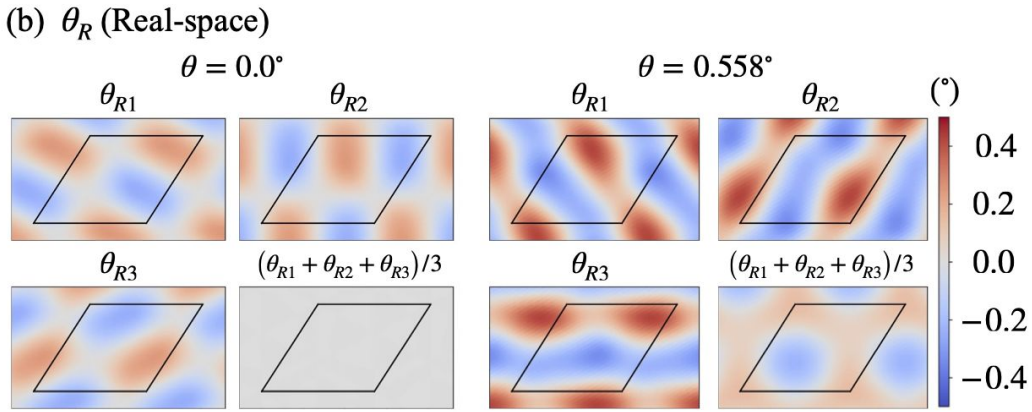

Understanding the primary gap increase: local rotation angle

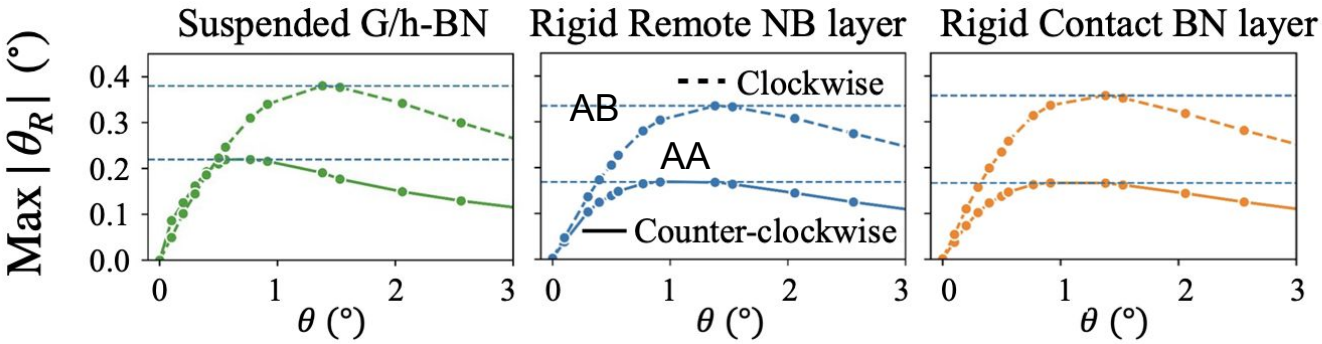

Increased local rotation at the AA (counter-clockwise) and AB stacking (clockwise) matches the larger lattice reconstruction for these angles.

Energetic stability?

Energetic stability

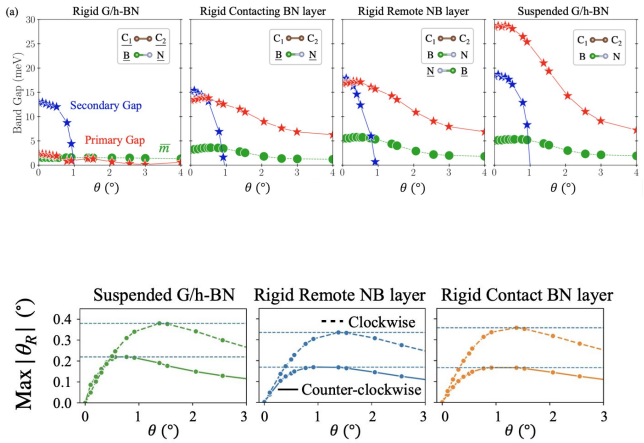

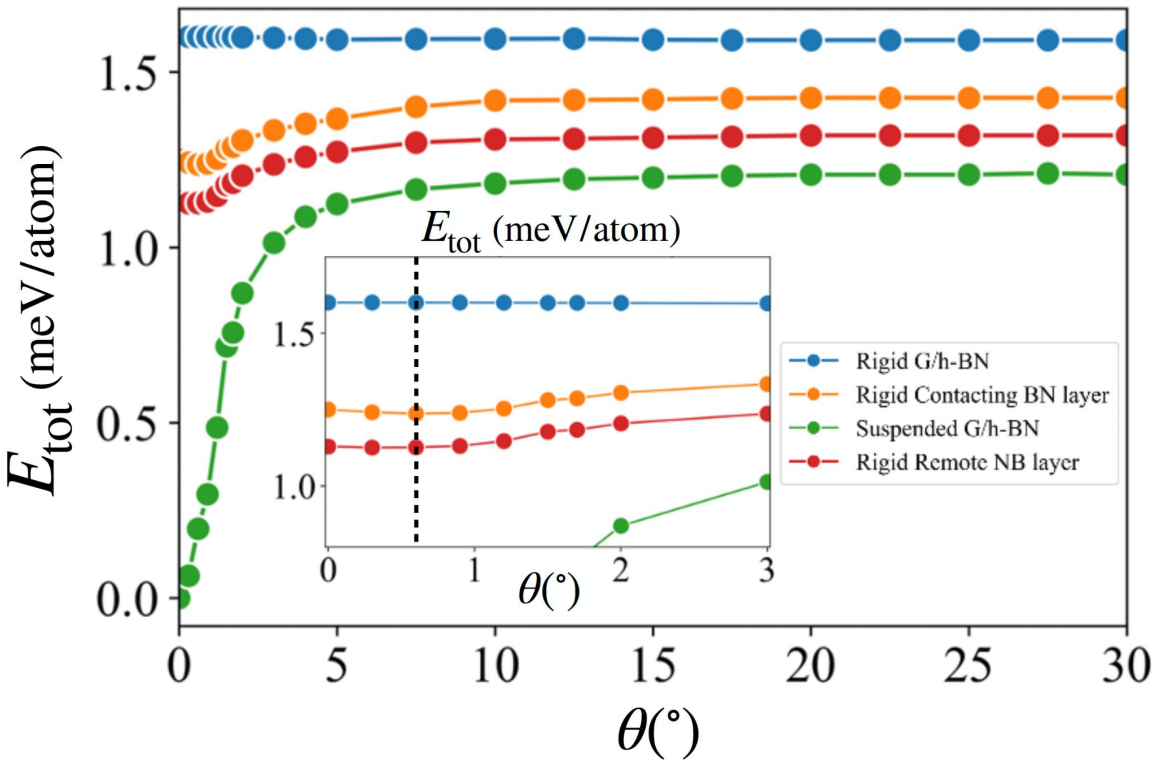

Large angle regime: robust 1 meV gap up to 30 degree

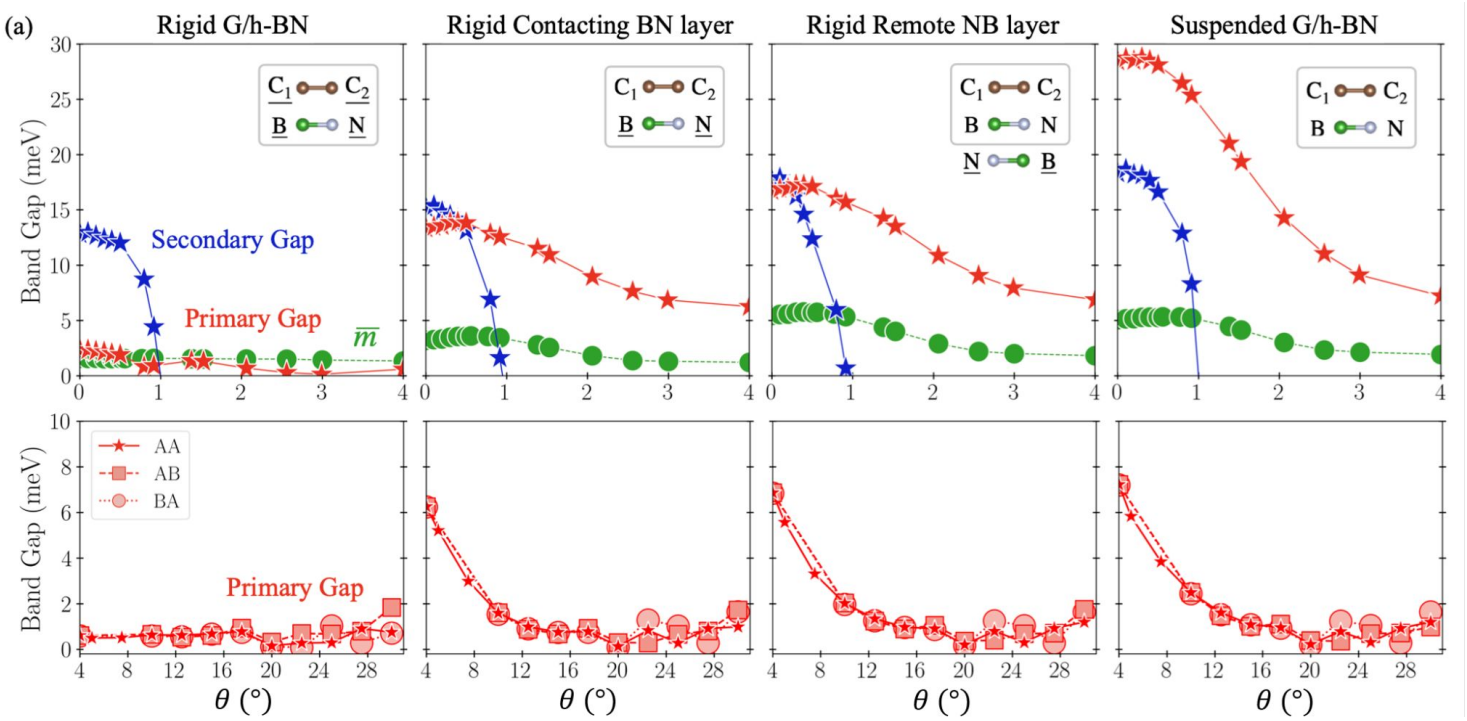

Take-home messages

- Substrate reduces the amplitude of the primary and secondary gaps in G-hBN
- Substrate causes larger lattice reconstruction away from perfect alignment
- Robust primary gap at large angle

Atomistic calculations of band gaps in graphene on hexagonal boron nitride

Jiaqi An,[1,2] Nicolas Leconte,[1] Srivani Javvaji,[1] Youngju Park,[1] and Jeil Jung[1,2,*]

[1]*Department of Physics, University of Seoul, Seoul 02504, Korea*

[2]*Department of Smart Cities, University of Seoul, Seoul 02504, Korea*

Charge transfer in h-BN encapsulated BG

Motivations

interfacial ferroelectricity by stacking non-polar materials in a symmetry-breaking way

Unconventional ferroelectricity in moiré heterostructures

Zhiren Zheng, Qiong Ma, Zhen Bi, Sergio de la Barrera, Ming-Hao Liu, Nannan Mao, Yang Zhang, Natasha Kiper, Kenji Watanabe, Takashi Taniguchi, Jing Kong, William A. Tisdale, Ray Ashoori, Nuh Gedik, Liang Fu, Su-Yang Xu & Pablo Jarillo-Herrero

Nature **588**, 71–76 (2020) | Cite this article

Giant ferroelectric polarization in a bilayer graphene heterostructure

Ruirui Niu, Zhuoxian Li, Xiangyan Han, Zhuangzhuang Qu, Dongdong Ding, Zhiyu Wang, Qianling Liu, Tianyao Liu, Chunrui Han, Kenji Watanabe, Takashi Taniguchi, Menghao Wu, Qi Ren, Xueyun Wang, Jiawang Hong, Jinhai Mao, Zheng Han, Kaihui Liu, Zizhao Gan & Jianming Lu

Nature Communications **13**, Article number: 6241 (2022) | Cite this article

arXiv > cond-mat > arXiv:2102.12398

Condensed Matter > Mesoscale and Nanoscale Physics

[Submitted on 24 Feb 2021]

Tunable ferroelectricity in hBN intercalated twisted double-layer graphene

Yibo Wang, Siqi Jiang, Jingkuan Xiao, Xiaofan Cai, Di Zhang, Ping Wang, Guodong Ma, Yaqing Han, Jiabei Huang, Kenji Watanabe, Takashi Taniguchi, Alexander S. Mayorov, Geliang Yu

Electric field tunable layer polarization in graphene/boron-nitride twisted quadrilayer superlattices

Ziyan Zhu, Stephen Carr, Qiong Ma, and Efthimios Kaxiras
Phys. Rev. B **106**, 205134 – Published 21 November 2022

An atomistic approach for the structural and electronic properties of twisted bilayer graphene-boron nitride heterostructures

Min Long, Pierre A. Pantaleón, Zhen Zhan, Francisco Guinea, Jose Ángel Silva-Guillén & Shengjun Yuan

npj Computational Materials **8**, Article number: 73 (2022) | Cite this article

arXiv > cond-mat > arXiv:2211.16351

Condensed Matter > Mesoscale and Nanoscale Physics

[Submitted on 29 Nov 2022]

Strong gate-tunability of flat bands in bilayer graphene due to moiré encapsulation between hBN monolayers

Robin Smeyers, Lucian Covaci, Milorad V. Milošević

Types of system

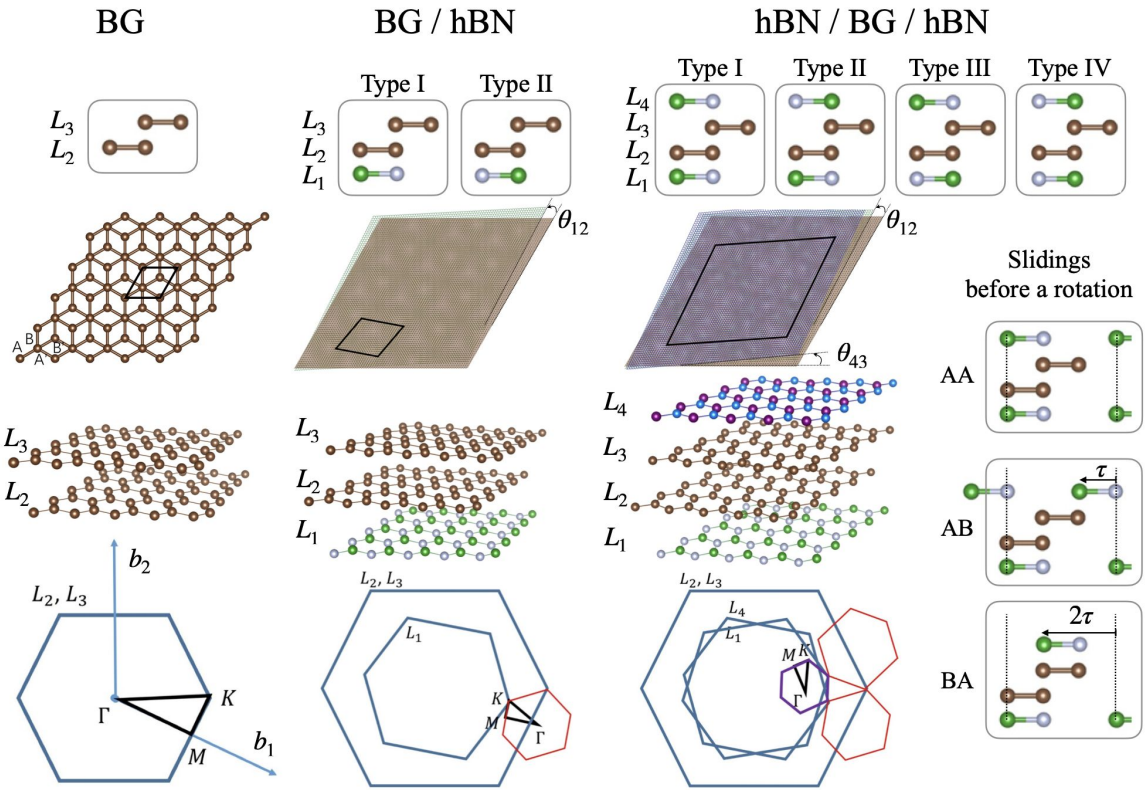

Charge transfer in BG on hBN

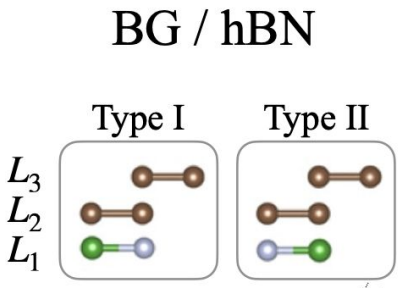

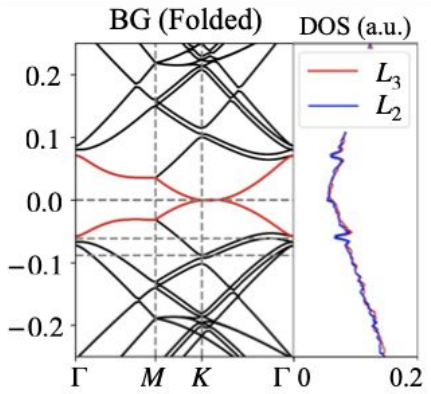

No charge transfer

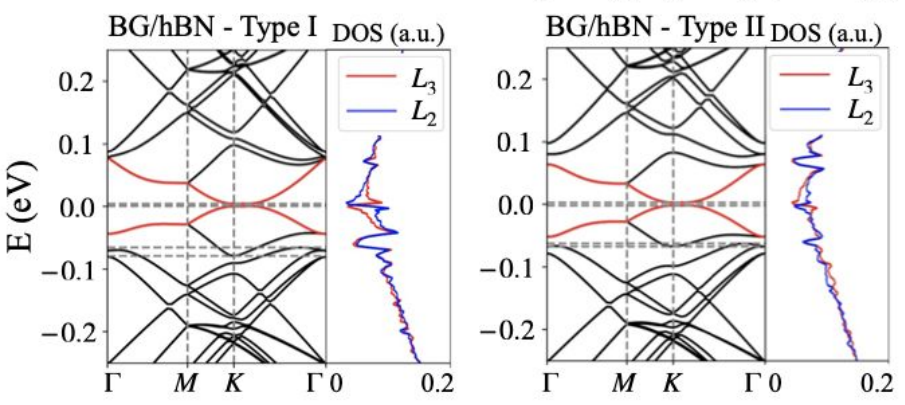

Larger charge on contacting G layer

Larger charge on remote G layer

Charge transfer in encapsulated systems

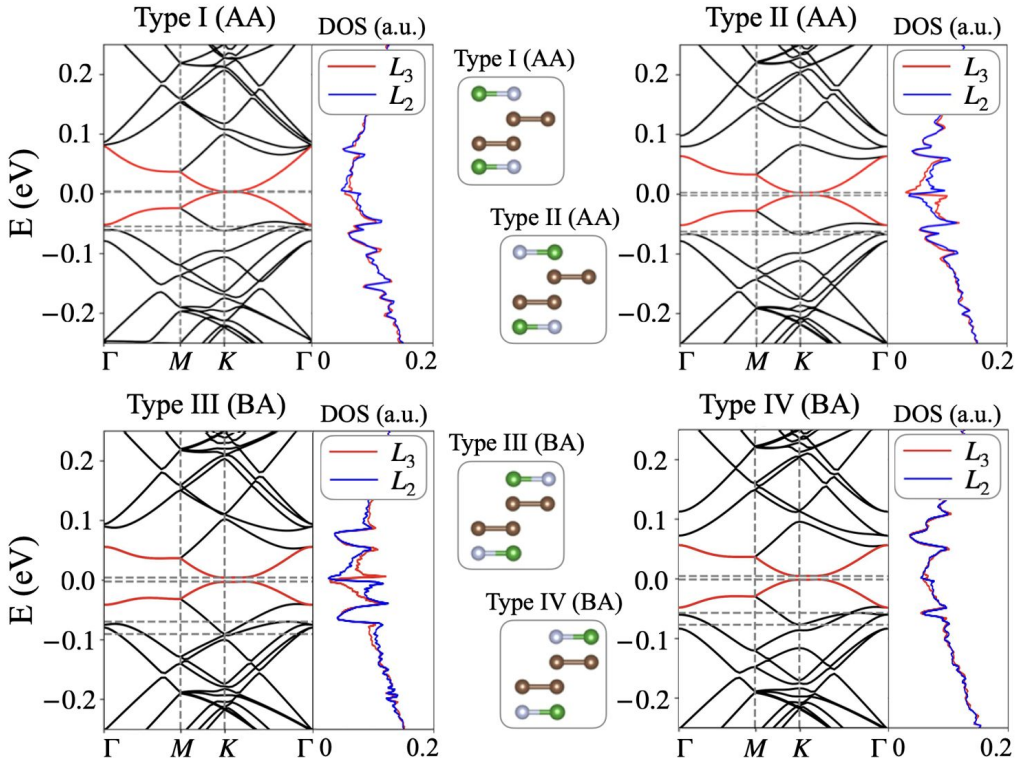

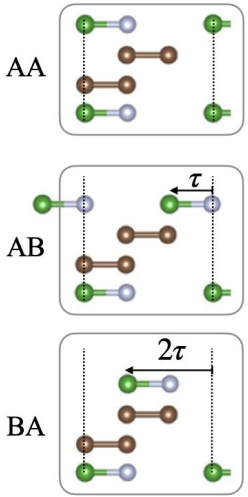

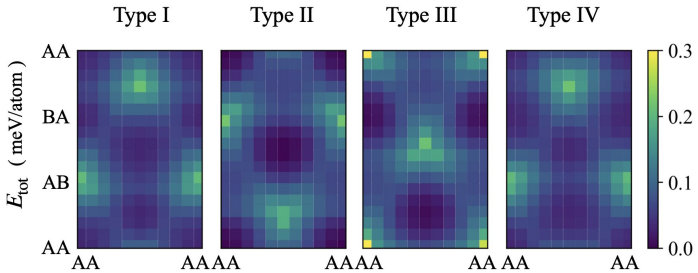

Energetic stability

Sliding-dependence of the charge transfer

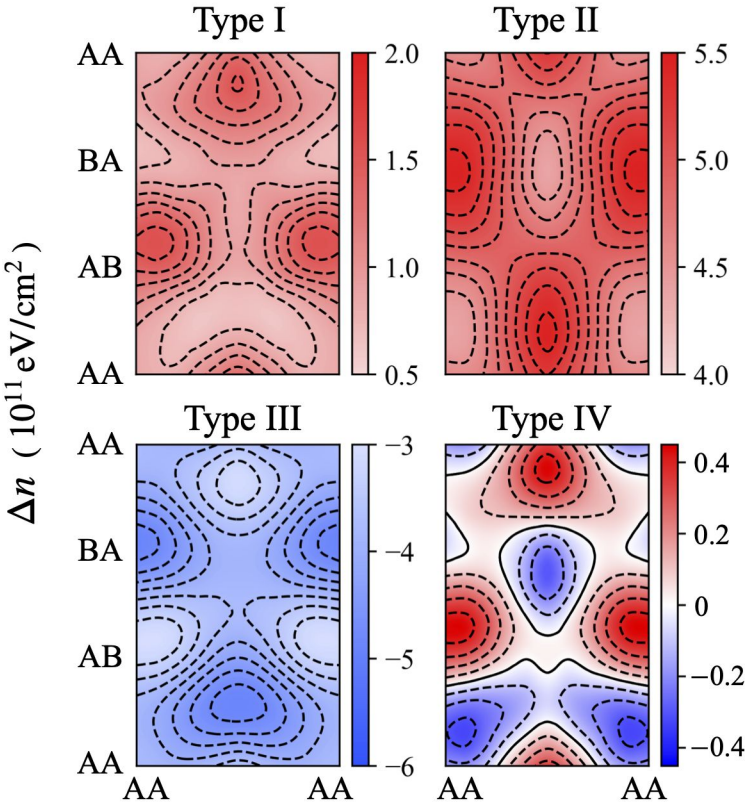

$$\Delta n = n_{L_3} - n_{L_2} \ [\mathrm{eV/cm^2}]$$

Red: more charge on layer 2

Blue: more charge on layer 3

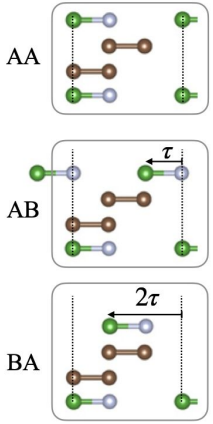

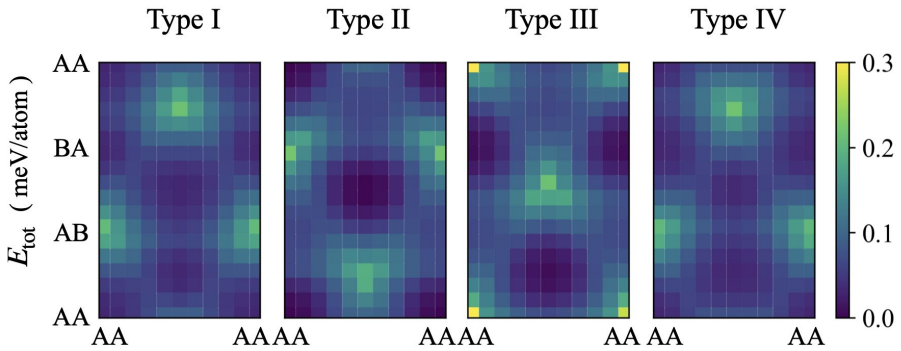

Shared colormap range…

Red: more charge on layer 2

Blue: more charge on layer 3

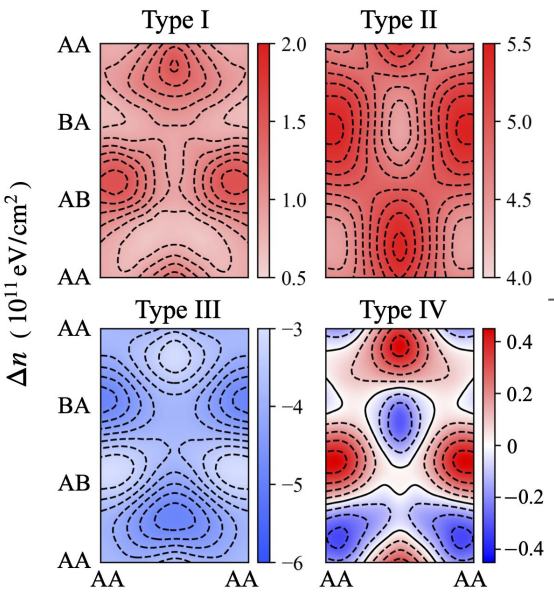

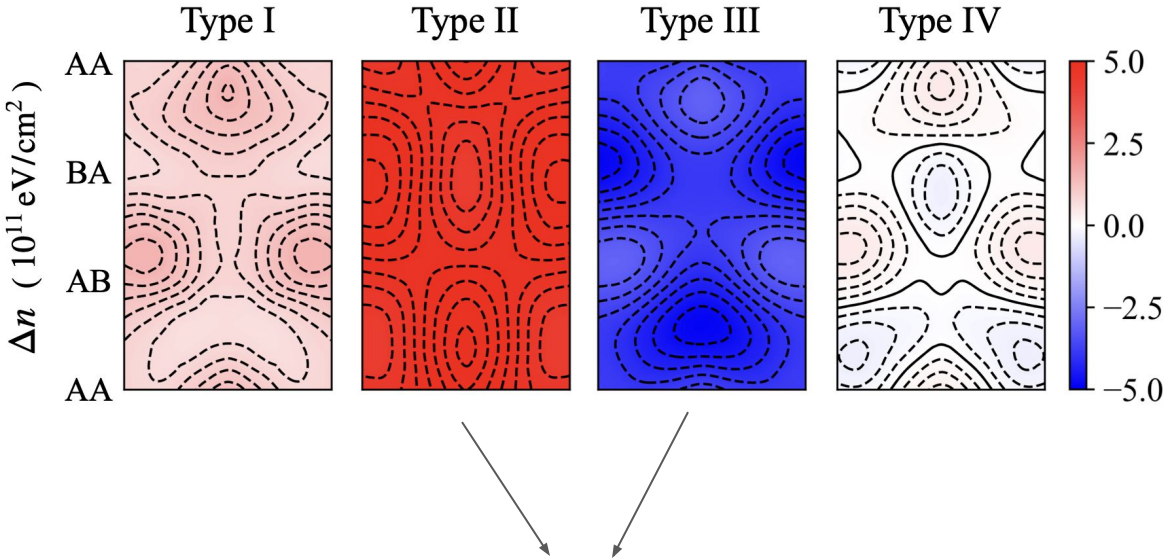

Largest charge transfer

Understanding…

Red: more charge on layer 2

Blue: more charge on layer 3

BG / hBN

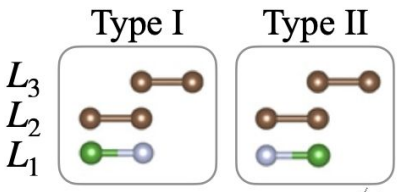

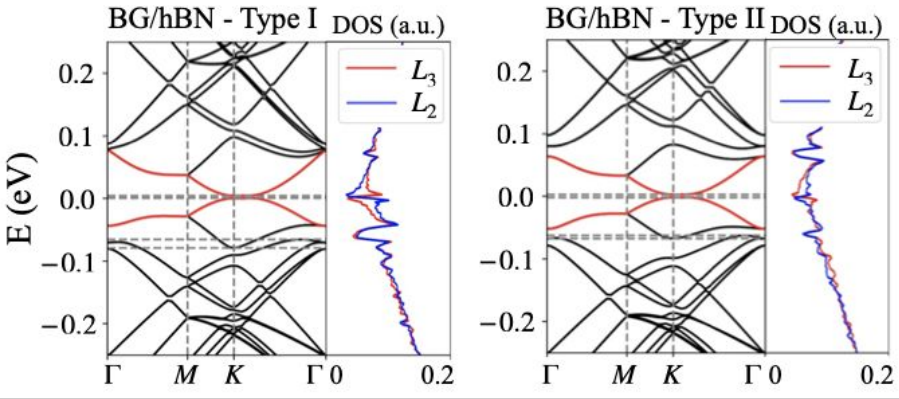

hBN / BG / hBN

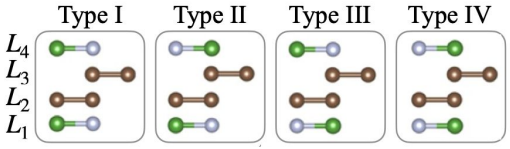

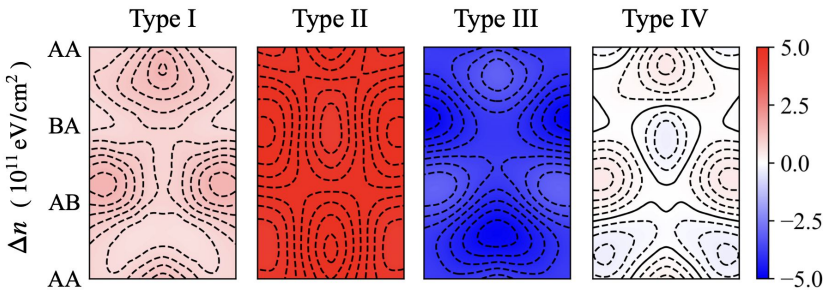

Effect of rotation

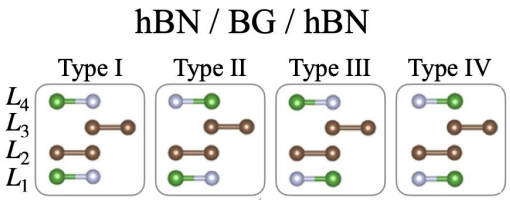

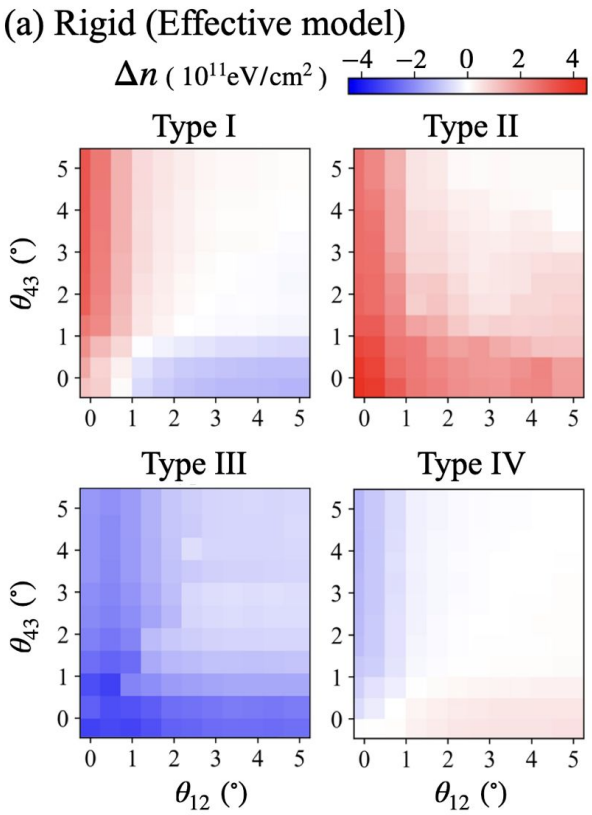

- Twisting away from alignment: decoupling between layers
- At 5 degree, hBN barely has a charging effect
- Behavior is explained by respective contribution of individual hBN layers

Red: more charge on layer 2

Blue: more charge on layer 3

Effect of relaxation

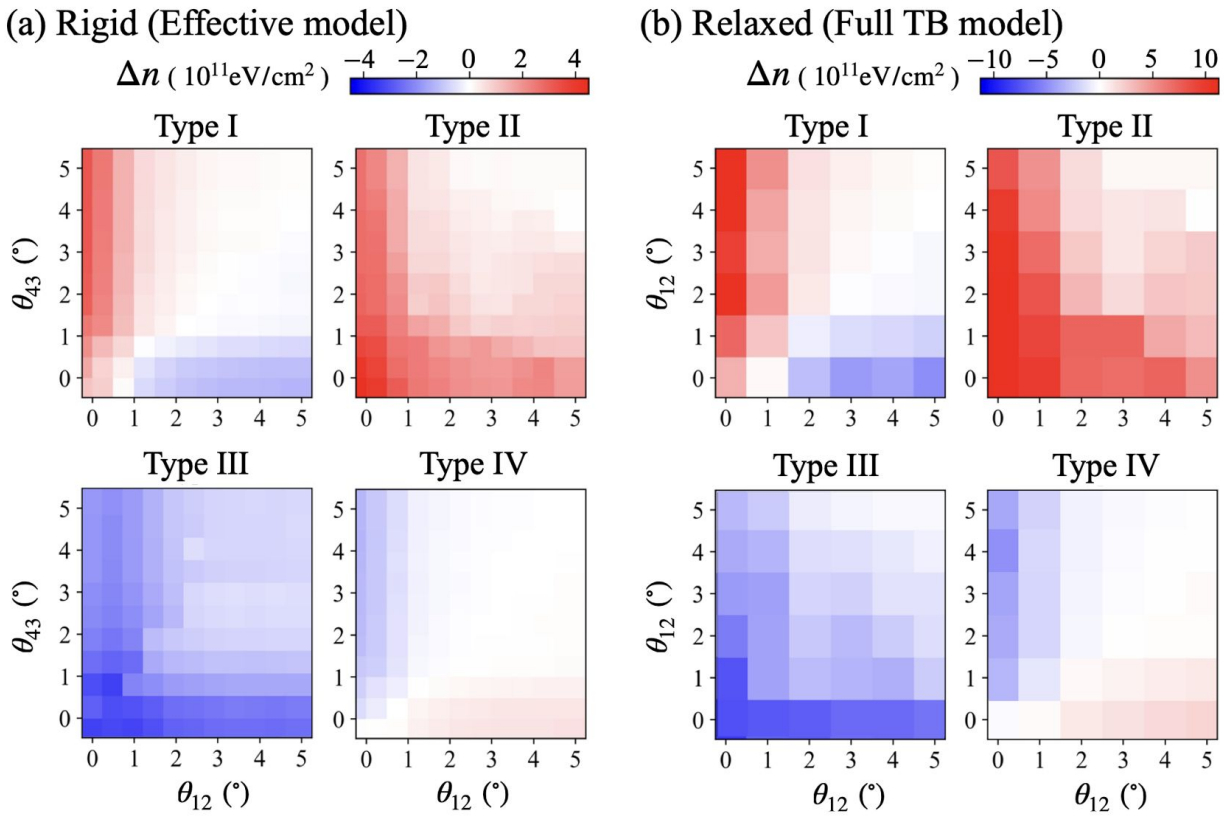

Factor 2.5 increase in charge transfer

Take home message

Charge transfer from double moire can mostly be understood from single moire charge transfer contributions

Layer Polarization and Charge Transfer in h-BN Encapsulated Bilayer Graphene

Jiaqi An,[1] Nicolas Leconte,[1] Youngju Park,[1] Appalakondaiah Samudrala,[1] and Jeil Jung[1]

[1] *Department of Physics, University of Seoul, Seoul 02504, Korea*

Conclusions

- The more accurate the force-field and tight-binding model parametrization, the better the quantitative comparison with experiment
- Lattice reconstruction affects the analytically predicted magic angles in tNG
- Substrate affects the primary and secondary angle-dependent gaps in G-hBN
- Charge transfer in encapsulated BG can be modulated by aligning the hBN layers in a parallel or antiparallel manner
- Methodology easily applicable for other layered materials

Thank you for your attention.

Questions?

Continuum and TB models

Continuum

$$\mathcal{H}_{\boldsymbol{k}} = \begin{pmatrix} H_{\boldsymbol{k}}^{-} & T(\boldsymbol{r}) & 0 & \cdots \\ T^{\dagger}(\boldsymbol{r}) & H_{\boldsymbol{k}'}^{+} & T^{\dagger}(\boldsymbol{r}) & \cdots \\ 0 & T(\boldsymbol{r}) & H_{\boldsymbol{k}}^{-} & \\ \vdots & \vdots & \vdots & \ddots \end{pmatrix} + \Delta\epsilon$$

$$H_{\boldsymbol{k}}^{\pm} = \hbar v_F \begin{pmatrix} 0 & \pi_{\boldsymbol{k}}^{\dagger} e^{\mp i\theta/2} \\ \pi_{\boldsymbol{k}} e^{\pm i\theta/2} & 0 \end{pmatrix}$$

$$\pi_{\boldsymbol{k}} = \bar{\boldsymbol{k}}_x + i\bar{\boldsymbol{k}}_y$$

$$T(\boldsymbol{r}) = \sum_{j=0,\pm} e^{-i\boldsymbol{Q}_j\cdot\boldsymbol{r}} \left[\begin{pmatrix} \omega' & \omega\, e^{-i\phi_j} \\ \omega\, e^{i\phi_j} & \omega' \end{pmatrix} e^{-i\boldsymbol{G}_j\cdot\boldsymbol{\tau}_s} \right]$$

bulk

$$\mathcal{H}_{\boldsymbol{k}}(k_z) = \begin{pmatrix} H_{\boldsymbol{k}}^{-} & 2T(\boldsymbol{r})\cos(k_z c_0) \\ 2T^{\dagger}(\boldsymbol{r})\cos(k_z c_0) & H_{\boldsymbol{k}'}^{+} \end{pmatrix}$$

$$\Delta\epsilon = \mathrm{diag}\left(-\frac{N-1}{2}, -\frac{N-1}{2}+1, \ldots, +\frac{N-1}{2}\right) \cdot \frac{\Delta V}{N-1}\mathbb{1}$$

Tight-binding

$$\hat{H} = \sum_i^{n_{at}} \epsilon_i |i\rangle\langle i| + \sum_{i,j}^{n_{at}} t_{ij} |i\rangle\langle j| \qquad |k\rangle = \frac{1}{\sqrt{n_{at}}} \sum_j^{n_{at}} e^{i\boldsymbol{k}\cdot\boldsymbol{r}_j} |j\rangle$$

$$t_{ij} = t_{ij}^{\mathrm{intra}} + t_{ij}^{\mathrm{inter}}$$

F2G2

arXiv:1910.12805

$$t_{ij}^{\mathrm{inter}} = S \exp\left[\frac{c_{ij} - p}{q}\right] t_{\mathrm{TC},ij}^{\mathrm{inter}}$$

$$t_{\mathrm{TC},ij} = V_{pp\pi}(r_{ij})\left[1 - \left(\frac{c_{ij}}{r_{ij}}\right)^2\right] + V_{pp\sigma}(r_{ij})\left(\frac{c_{ij}}{r_{ij}}\right)^2$$

$$V_{pp\pi}(r_{ij}) = V_{pp\pi}^0 \exp\left(-\frac{r_{ij} - a_0}{r_0}\right)$$

$$V_{pp\sigma}(r_{ij}) = V_{pp\sigma}^0 \exp\left(-\frac{r_{ij} - c_0}{r_0}\right)$$

$$S = \frac{\theta_1 |t_{\mathrm{eff}}|}{\omega} s = C_1 s$$

Understanding charge distribution

k=2, states are on outer layers, thus weaker angle reduction effects

Separate tNG multilayer Hamiltonian into smaller subsystems using basis of odd layer symmetric or even layer antisymmetric wave functions based on the eigenstates of opposite sign eigenvalues $\lambda_k = -\lambda_{N+1-k}$

$$|\tilde{\psi}_k^{\text{odd}}\rangle = \frac{|\psi_k\rangle + |\psi_{N+1-k}\rangle}{\sqrt{2}},$$

$$|\tilde{\psi}_k^{\text{even}}\rangle = \frac{|\psi_k\rangle - |\psi_{N+1-k}\rangle}{\sqrt{2}}.$$

$$|\psi_k\rangle \qquad k = 1, 2, \cdots, N_e$$

$$\psi_k(\ell) \qquad \ell = 1, 2, \ldots, N$$

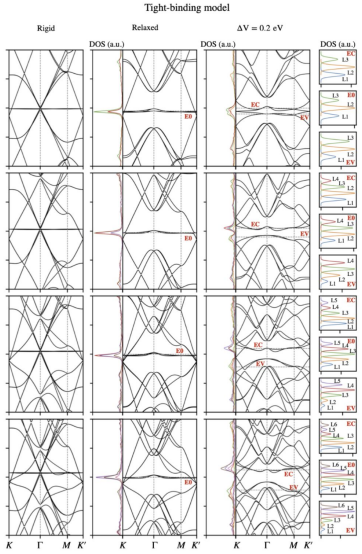

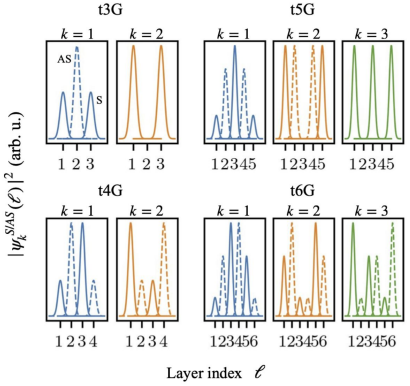

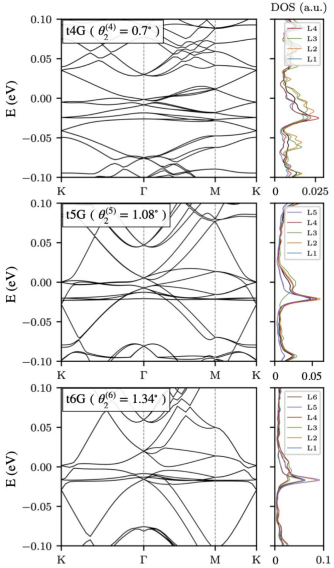

Magneto-optical properties of multilayer graphene

Mikito Koshino and Tsuneya Ando
Phys. Rev. B **77**, 115313 – Published 11 March 2008

Separation into elastic and potential energy maps

$$E_i^{\mathrm{el}} = \sum_{j \in \text{layer i}} \phi_{ij} \tag{A.1}$$

$$E_i^{\mathrm{pot}} = \sum_{j \notin \text{layer i}} \phi_{ij} = \sum_{j \in \text{ any layer}} \phi_{ij} - E_i^{\mathrm{el}} \tag{A.2}$$

Extracted from LAMMPS:

- Get the atom-resolved energy maps
- Separate into elastic (only in-plane interactions) and potential (only out-of-plane pairwise interactions) during post-processing

t3G maps

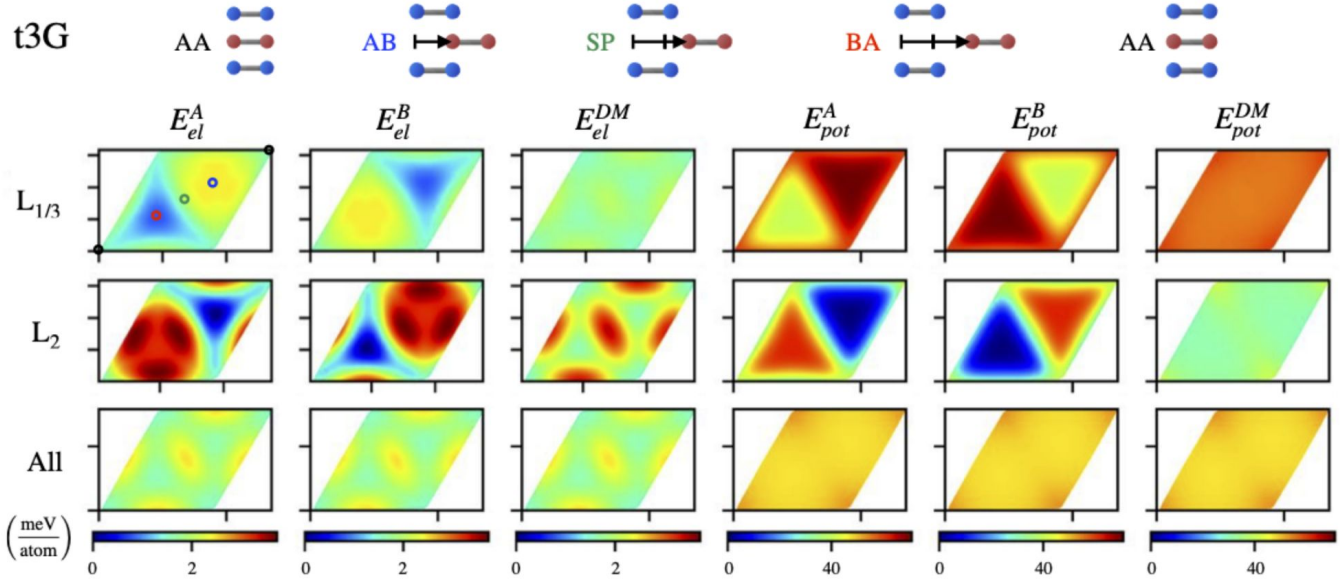

- Layer and sublattice-resolved contributions
- Order of magnitude larger potential energy contribution: energetically favorable regions can be fully inferred from the potential energy
- Elastic energy shows the largest contributions in the SP regions when adding up all layer contributions
- L2 shows twice as large contributions compared to L1 and L3
- Chiral signatures are observed (add Ref 35, 36)

t4G maps

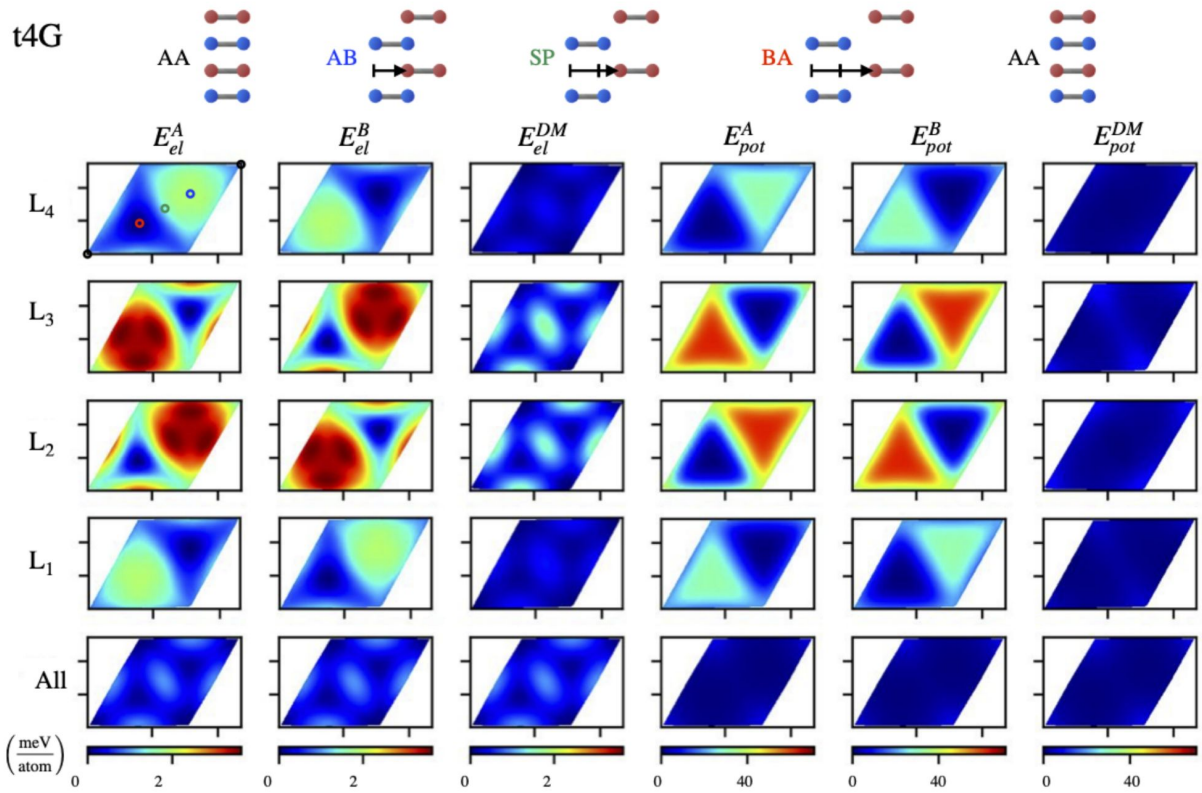

For increasing N, the trends can be inferred from N=3 and N=4 maps.

Magic angle predictions: explanations

- Remember: stronger coupling implies larger magic angle
- Largest drop for bulk: decreased coupling?
- Yes: distance increases from 3.313 Ang (AB stacked) to 3.328 Ang for bulk system at 2 degree. Why?
- Increasing AA contribution/weakening AB contribution for larger angle (weaker lattice reconstruction), increased estimates for average interlayer distance:

$$\bar{c}_{ij}^{\text{bulk}} = r_{\text{AA}} c_0^{\text{AA}} + r_{\text{AB/BA}} c_0^{\text{AB/BA}} + r_{\text{SP}} c_0^{\text{SP}}$$

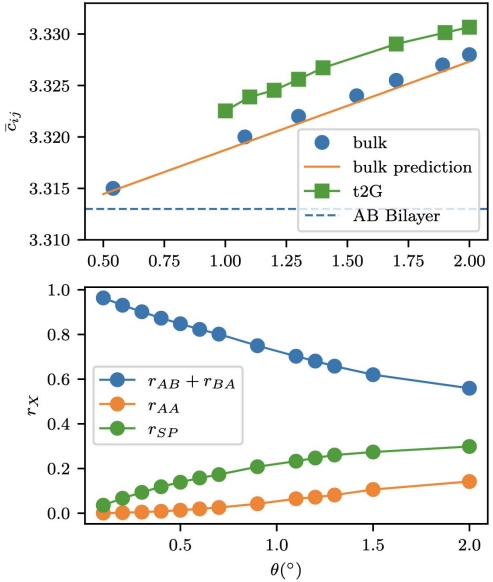

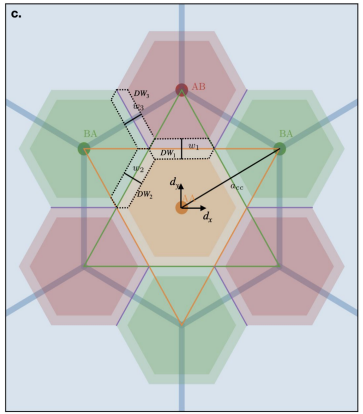

Magic angle predictions: explanations

- N-dependence of average interlayer distance: converges to bulk value with increasing N
- Monotonic decrease for fixed outer layers (no out-of-plane relaxation)
- Gradual convergence when allowing for out-of-plane relaxation in case of free-standing configuration
- Minimum average distance at N=14 agrees with observed maximum angle for N=10
- Open question: how many layers to recover bulk behavior?

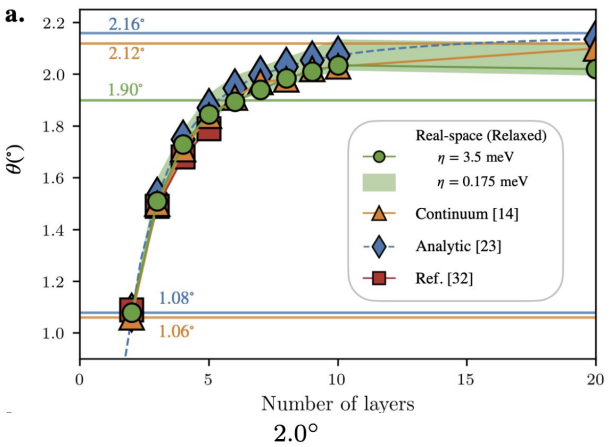

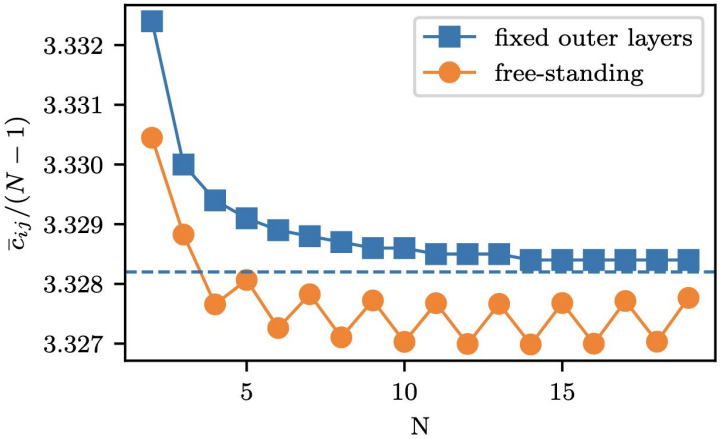

$$W_\Gamma = E_{\mathrm{cond}}(\Gamma) - E_{\mathrm{val}}(\Gamma)$$

$$\theta_{\mathrm{eff}} = \theta_{\mathrm{ref}} - \delta\theta = \frac{S}{S'}\theta_{\mathrm{ref}}$$

$$S = \frac{\theta_1 |t_{\mathrm{eff}}|}{\omega} s = C_1 s$$

$$S' = C_1' s = C_1 \left(1 + \frac{\delta\theta}{\theta_{\mathrm{ref}}}\right)\left(1 + \frac{\delta\upsilon_{\mathrm{F}}}{\upsilon_{\mathrm{F}}}\right)\left(\frac{\omega}{\omega + \delta\omega}\right) s.$$

Electronic band structures up to N=6

- Modify S' to get the bandstructure for effective angle using reference commensurate angle
- Minimize band-width at Gamma
- Relaxation effect: el-hole asymmetry, separation of high energy bands from low energy bands at Gamma
- States are mostly located on the inner layers
- Layer asymmetry in DOS when applying electric field
- E-field: gap in the case of t4G

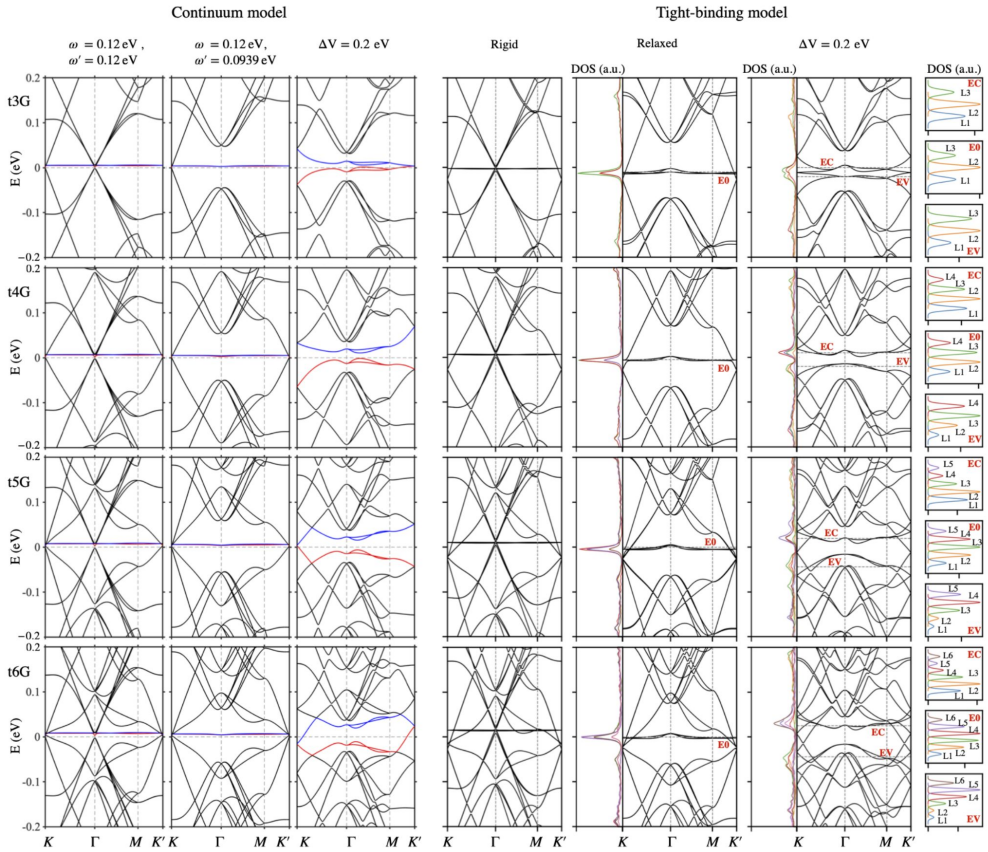

Bulk mapping

Analogy with 1d-chain

$$k_z c_0 = \frac{\pi k}{N+1}$$

$$N = 8$$

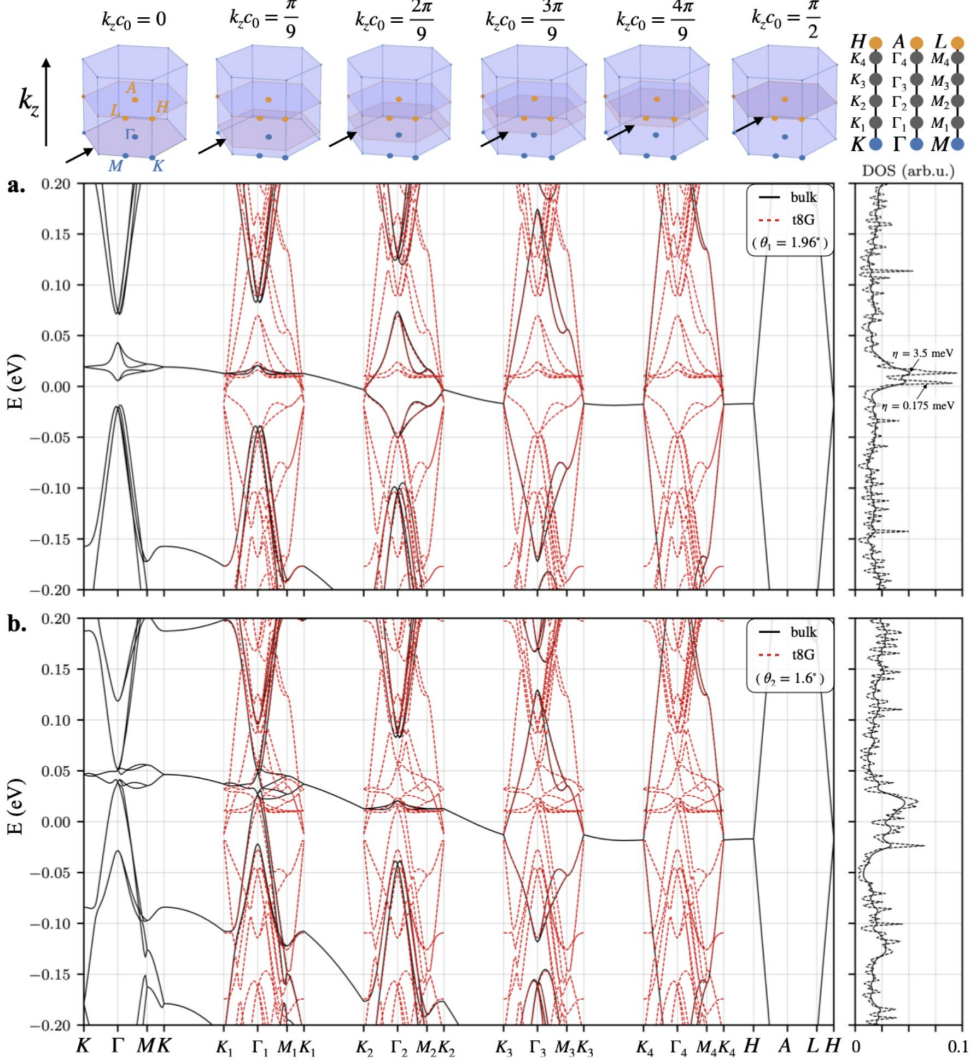

$$\lambda_k = 2\cos(\kappa_k),$$

$$\psi_k(\ell) = \sqrt{\frac{2}{N+1}}\sin(\kappa_k\,\ell)$$

$$k = 1, 2, \cdots, N_e.$$

$\ell = 1, 2, \ldots, N$ are the layer indices.

$$\kappa_k = \pi k/(N+1)$$

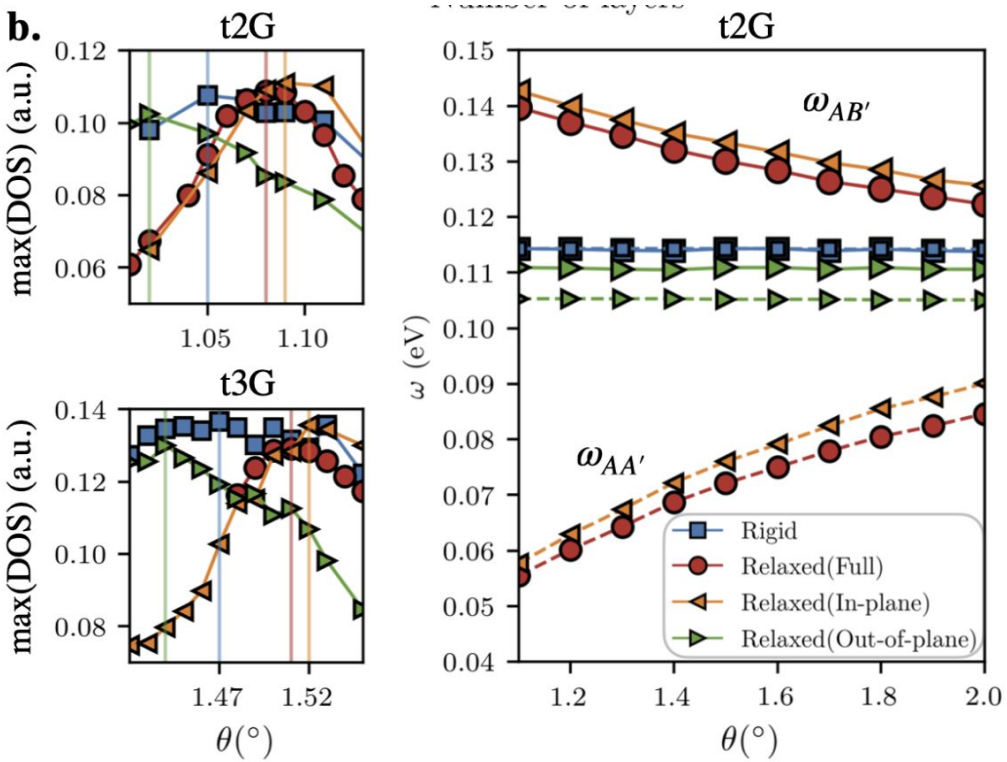
b.
t2G
max(DOS) (a.u.)
0.12
0.10
0.08
0.06
1.05
1.10
t3G
max(DOS) (a.u.)
0.14
0.12
0.10
0.08
1.47
1.52
θ(°)
t2G
ω (eV)
0.15
0.14
0.13
0.12
0.11
0.10
0.09
0.08
0.07
0.06
0.05
0.04
ω_AB′
ω_AA′
Rigid
Relaxed(Full)
Relaxed(In-plane)
Relaxed(Out-of-plane)
1.2
1.4
1.6
1.8
2.0
θ(°)

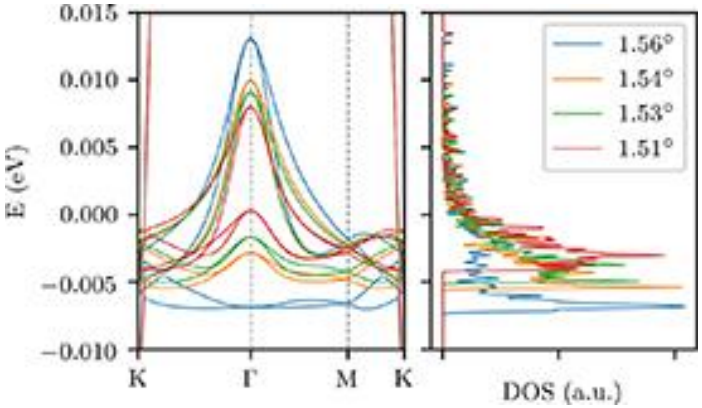
E (eV)
0.015
0.010
0.005
0.000
−0.005
−0.010
K
Γ
M
K
DOS (a.u.)
1.56°
1.54°
1.53°
1.51°

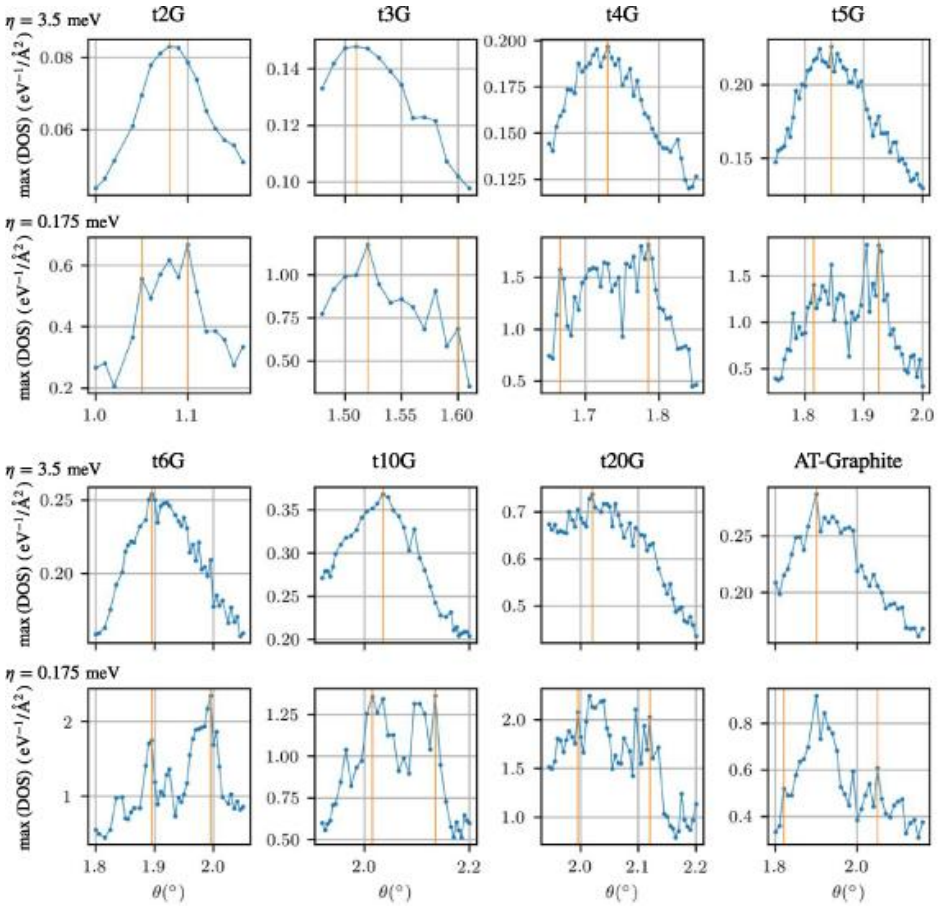
t2G
t3G
t4G
t5G
t6G
t10G
t20G
AT-Graphite
η = 3.5 meV
η = 0.175 meV
max (DOS) (eV⁻¹/Å²)
θ(°)